Jens Melder, Peter Bogdanoff, Ivelina Zaharieva,
Sebastian Fiechter*, Holger Dau* and Philipp Kurz*

Water-Oxidation Electrocatalysis by Manganese Oxides: Syntheses, Electrode Preparations, Electrolytes and Two Fundamental Questions

https://doi.org/10.1515/zpch-2019-1491
Received May 31, 2019; accepted November 26, 2019

Abstract: The efficient catalysis of the four-electron oxidation of water to molecular oxygen is a central challenge for the development of devices for the production of solar fuels. This is equally true for artificial leaf-type structures and electrolyzer systems. Inspired by the oxygen evolving complex of Photosystem II, the biological catalyst for this reaction, scientists around the globe have investigated the possibility to use manganese oxides ("MnO_x") for this task. This perspective article will look at selected examples from the last about 10 years of research in this field. At first, three aspects are addressed in detail which have emerged as crucial for the development of efficient electrocatalysts for the anodic oxygen evolution reaction (OER): (1) the structure and composition of the "MnO_x" is of central importance for catalytic performance and it seems that amorphous, $Mn^{III/IV}$ oxides with layered or tunnelled structures are especially good choices; (2) the type of support material (e.g. conducting oxides or nanostructured carbon) as well as the methods used to immobilize the MnO_x catalysts on them greatly influence OER overpotentials, current densities and long-term stabilities of the

***Corresponding authors: Sebastian Fiechter,** Helmholtz-Zentrum Berlin für Materialien und Energie GmbH, Institute for Solar Fuels, 14109 Berlin, Germany, e-mail: fiechter@helmhotz-berlin.de; **Holger Dau,** Freie Universität Berlin, Fachbereich Physik, Arnimallee 14, 14195 Berlin, Germany, e-mail: holger.dau@fu-berlin.de; and **Philipp Kurz,** Institut für Anorganische und Analytische Chemie und Freiburger Materialforschungszentrum (FMF), Albert-Ludwigs-Universität Freiburg, Albertstraße 21, 79104 Freiburg, Germany, e-mail: philipp.kurz@ac.uni-freiburg.de
Jens Melder, Institut für Anorganische und Analytische Chemie und Freiburger Materialforschungszentrum (FMF), Albert-Ludwigs-Universität Freiburg, Albertstraße 21, 79104 Freiburg, Germany
Peter Bogdanoff, Helmholtz-Zentrum Berlin für Materialien und Energie GmbH, Institute for Solar Fuels, 14109 Berlin, Germany
Ivelina Zaharieva, Freie Universität Berlin, Fachbereich Physik, Arnimallee 14, 14195 Berlin, Germany

electrodes and (3) when operating MnO_x-based water-oxidizing anodes in electrolyzers, it has often been observed that the electrocatalytic performance is also largely dependent on the electrolyte's composition and pH and that a number of equilibria accompany the catalytic process, resulting in "adaptive changes" of the MnO_x material over time. Overall, it thus has become clear over the last years that efficient and stable water-oxidation electrolysis by manganese oxides can only be achieved if at least four parameters are optimized in combination: the oxide catalyst itself, the immobilization method, the catalyst support and last but not least the composition of the electrolyte. Furthermore, these parameters are not only important for the electrode optimization process alone but must also be considered if different electrode types are to be compared with each other or with literature values from literature. Because, as without their consideration it is almost impossible to draw the right scientific conclusions. On the other hand, it currently seems unlikely that even carefully optimized MnO_x anodes will ever reach the superb OER rates observed for iridium, ruthenium or nickel-iron oxide anodes in acidic or alkaline solutions, respectively. So at the end of the article, two fundamental questions will be addressed: (1) are there technical applications where MnO_x materials could actually be the first choice as OER electrocatalysts? and (2) do the results from the last decade of intensive research in this field help to solve a puzzle already formulated in 2008: "*Why did nature choose manganese to make oxygen*?".

Keywords: artificial photosynthesis; electrocatalysis; manganese oxides; water-oxidation.

1 Introduction

The development of an affordable, environmentally friendly and CO_2-neutral energy supply is one of the greatest social and scientific challenges mankind is facing today. The search for suitable ways to store the energy of abundant renewable sources like sunlight, wind or geothermal heat is closely associated with this problem. A concept that has already been suggested over 100 years ago by Ciamician and which is still very high on the global research agenda is "artificial photosynthesis" or the production of so-called "solar fuels" [1–6]. In artificial photosynthesis sunlight is used to produce energy carriers or raw materials from abundant sources like water, CO_2 or N_2 [see Eq. (1)].

$$H^+ / CO_2 / N_2 + H_2O \xrightarrow[energy]{solar} H_2 / CH_4 / NH_3 + O_2 \quad (1)$$

Without copying the very high complexity of the biochemical machinery, artificial photosynthesis conceptually follows the blueprint of the biological photosynthetic reactions in plants or phototrophic microorganisms, where carbohydrates are biochemically synthesised from water and CO_2 using the energy of absorbed sunlight. Both artificial and biological photosynthesis involve two multi-electron redox reactions: one on the reductive side to produce the desired product (in the simplest case H_2 from H^+) and as second half-reaction the oxidation of water [Eq. (2)].

$$2\,H_2O_{(l)} \rightarrow O_{2(g)} + 4H^+_{(aq)} + 4e^- \tag{2}$$

This oxygen evolution reaction (OER) is often considered to be a major bottleneck of the overall process, as it is mechanistically very demanding due to the necessary transfers of four protons and four electrons accompanying the formation of one oxygen molecule [7, 8]. The minimum potential necessary to drive this reaction is +1.23 V vs. the reversible hydrogen electrode (RHE; note: all redox potentials in this article are given relative to the reversible hydrogen electrode), but commonly very large overpotentials η of >750 mV have to be applied to e.g. bare carbon electrodes to reach significant OER reaction rates. Thus, the development of efficient, affordable, abundant and non-toxic catalysts for water-oxidation catalysis (WOC) is a central task for the researchers in the field of artificial photosynthesis, but also in related areas like power-to-X technologies [9–13].

In biological photosynthesis, reaction (2) is catalyzed by the oxygen evolving complex (OEC), a $Mn_4CaO_5(H_2O)_x$-cluster embedded in the multi-subunit membrane-bound enzyme Photosystem II (PS II). With it biology provides a template for a highly efficient water oxidation catalyst in neutral media (TOF of about 300 $O_2\,s^{-1}$ at $\eta = \sim$300 mV and pH 5.5 [14]) composed only of earth-abundant elements (Mn, O and Ca) [15–18]. The accumulation of the four oxidation equivalents needed according to Eq. (2) is mainly accomplished by Mn ions switching between the oxidation states +III and +IV coupled to deprotonation steps of coordinated water molecules or hydroxide ions [19, 20]. For a more detailed discussion of key structural features of the OEC and its mechanism of WOC, please refer to Figure 13 and the final section of this article.

Inspired by nature many attempts to the synthesis of molecular model complexes or related structures for the OEC with the aim to develop a synthetic molecular Mn-based catalyst for water oxidation have been undertaken [21–31]. Such model systems are important for the understanding of natural photosynthesis. For example, direct measurements and major chemical variations of redox potentials and proton binding energies, alternative mechanistic pathways and spectroscopic

characteristics of the OEC can be mimicked by such complexes. However, due to low water oxidation activities and poor stabilities, molecular manganese catalysts are currently not suitable for a technological application. Instead, the clear champions for molecular water oxidation catalysis (WOC) are based on Ru and Ir [32].

Despite, manganese oxides (MnO_x) have been used as bio-inspired catalysts for heterogeneous water oxidation since the early 1960s when researcher from Kiev first reported the evolution of oxygen from aqueous suspensions of MnO_2 in the presence of Ce^{4+} [33–35]. First experiments with MnO_x as electrocatalyst for OER were carried out around 1980 by two independent groups from Japan and Italy [36, 37]. To date, much progress has been made in the field of heterogeneously catalysed water oxidation based on manganese oxides. This perspective article aims to provide insights into the developments in this field over the last decade, starting with a short overview on the rich structural variety of MnO_x materials and their use in (photo)chemical WOC. The major focus is then laid on electrochemical water oxidation using MnO_x-coated electrodes, for which the employed conductive substrate, the electrode preparation technique and parameters like the electrolyte or its pH on the activity and stability of such anodes are summarized. In the end, the article will try to answer two fundamental questions on the basis of our current understanding of WOC by manganese oxides: (1) are there realistic technological applications for MnO_x in artificial photosynthesis and (2) why did nature "choose" manganese as redox active component of the OEC?

2 Manganese oxides: structures and (photo)chemical water oxidation catalysis

More than 30 different manganese oxides/(oxy)hydroxides of different compositions and structural motifs are known to occur in the earth's crust [38]. Even though many of them contain additional elements besides manganese and oxygen, the term "MnO_x" is commonly used as a generalizing abbreviation for the entire class of compounds. In most manganese oxide minerals, Mn occurs in the oxidation states +II, +III and/or +IV and the manganese ions are usually coordinated by six water-derived ligands (WDL, i.e. O^{2-} / OH^- / H_2O). Depending on the connectivity between these [MnO_6] building blocks, tunnelled (e.g. cryptomelane, pyrolusite, ramsdellite), layered (e.g. buserite, birnessite) or three-dimensional networks (e.g. bixbyite, hausmannite) can be formed (Figure 1). Many further MnO_x variations are possible as a number of alkaline, alkaline-earth

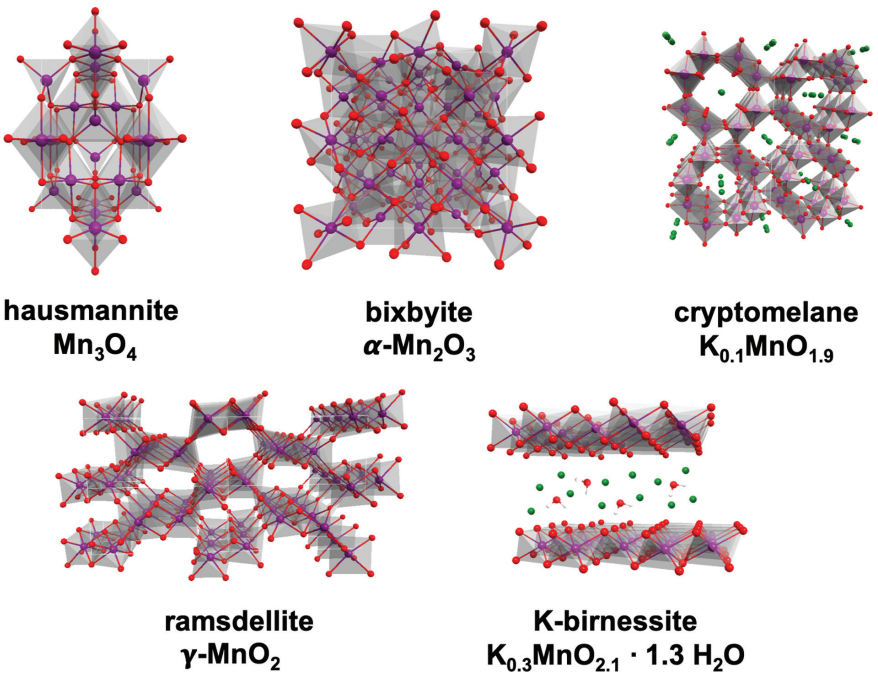

Fig. 1: Structures of selected manganese oxides (MnO_x) featuring different structural motifs (tunneled: cryptomelane, ramsdellite; network: Mn_3O_4, Mn_2O_3 and layered: birnessite). In each case the common [MnO_6]-building blocks are given in grey. Oxygen atoms are represented in red, manganese ions in purple and potassium ions in green.

and/or transition metals can be incorporated into these structures, especially into the tunnels or interlayer spaces. Comprehensive summaries of the different geologically occurring MnO_x can be found in the literature [38, 39], together with other reviews covering possible synthetic routes leading to the different classes of MnO_x together with a brief summary about structural parameters [35].

As a consequence of the growing interest in developing MnO_x for water-oxidation catalysis (but also for other energy-related applications like supercapacitors or batteries), numerous preparation methods for MnO_x have been developed and optimized [35, 38, 40, 41]. Over the last decade, a significant number of these oxides have then been tested as heterogeneous (electro-)chemical water-oxidation catalysts leading to a plethora of publications concerning WOC by MnO_x. Generally, such WOC screenings can be carried out photochemically oxidants (most often by using Ce^{4+} or $[Ru(bipy)_3]^{3+}$) or (photo)electrochemically (where the MnO_x is immobilized on an illuminated semiconductor or a conductive support material) [35, 42, 43]. Even though this article will mainly

address electrochemical WOC by MnO_x (in the dark), we will start with a short overview about MnO_x-based water oxidation catalysts tested in (photo)chemical systems.

Using the single-electron oxidation agents Ce^{4+} ($E\sim+1.6$ V; typical pH ~1–2) or $[Ru(bipy)_3]^{3+}$ ($E\sim+1.6$ V; typical pH ~4–8), it has been found that many MnO_x polymorphs are WOC-active. However, it has been noted in a number of screenings that the catalytic activities of the different polymorphs varies significantly. In attempts to find possible structure-activity relationships, Robinson et al. [44] for example tested eight different synthetic MnO_x polymorphs using $[Ru(bipy)_3]^{3+}$ as oxidant and concluded that MnO_x polymorphs featuring Mn^{3+} in edge-sharing octahedra are catalytically more active than Mn^{IV}-oxides. As possible reason the authors pointed to the weaker/longer (Jahn-Teller distorted) Mn^{III}-O bonds (in comparison to Mn^{IV}), which could lead to the high structural flexibility needed for a good water oxidation catalysis. MnIII-O-units might also involved in the formation of active surface layers during electrochemical water oxidation (see Section 3.4). In another study, one of our groups screened a dozen different MnO_x polymorphs for WOC using the sacrificial electron acceptor Ce^{4+} (Figure 2) [41, 45–48]. The tested materials were classified as 3D-networks, tunnelled or layered oxides. It was figured out, that especially amorphous tunnelled and layered MnO_x (e.g. todorokite, Ca-birnessite) showed the highest catalytic activities. This was explained by the high surface areas (determined by N_2 gas sorption measurements, Figure 2) and large pore or interlayer volumes of such materials, resulting in a good accessibility for water and highly flexible Mn–O–Mn linkages. Furthermore, we concluded that a good water oxidation catalyst must allow facile, reversible $Mn^{III} \rightleftharpoons Mn^{IV}$ oxidation state changes during operation within the given oxide structure – a feature we observed in particular for birnessites in a number of detailed investigations [49]. From these and further (photo)chemical studies by the groups of Harriman [50], Frei [51, 52], Spiccia [53] and others [33–35, 54–58], the following factors have in our opinion emerged as crucial "ingredients" for a good WOC-performance by MnO_x: (1) flexible structures are beneficial for substrate binding and oxidation changes of the Mn ions; (2) high surface areas are important for a good accessibility of the active sites; (3) average Mn-oxidation states $>\sim+3.7$ are most likely needed during operation in order to provide a sufficiently large driving force for the OER; (4) it is often beneficial if the oxide structure contains water molecules as well as weakly Lewis-acidic secondary cations.

Despite these general trends, it has to be mentioned that the previously described, very large structural, chemical and morphological diversity of manganese oxides and the many non-standardized screening methods have resulted in a situation where different research groups currently have identified different

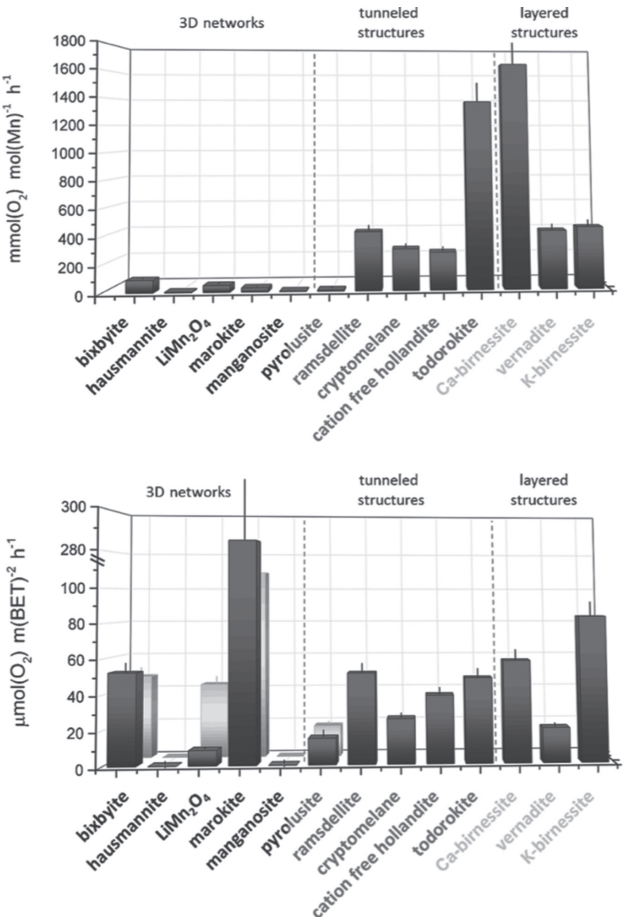

Fig. 2: Comparison of catalytic water oxidation rates for the different oxides with Ce^{4+} as oxidant. Top: Data normalised per mole of Mn. Bottom: Rates per unit surface area determined by N_2 physisorption (front row, black) or calculated from particle sizes (back row, grey). The error bars indicate the estimated 10% error of the absolute value. Reprinted from Ref. [41] with permission from John Wiley and Sons. Copyright ©2015 WILEY-VCH Verlag GmbH & Co. KGaA, Weinheim.

MnO_x as "winners" with respect to WOC activity. They also have come up with various suggestions for potential active sites where WOC might occur in MnO_x materials [48, 54, 55, 59]. Nevertheless, and as already outlined by some of us in 2015 [41], it seems that weakly-ordered tunneled (e.g. cryptomelane, hollandite, todorokite) or layered MnO_x (e.g. birnessite) seem to be especially suited to fulfill the four requirements for a good MnO_x-based water-oxidation catalyst listed

in the previous paragraph. However, the identification of such promising MnO_x candidates from the (photo)chemical screenings only marks a useful starting point, because as a next step, MnO_x-containing anodes have to be developed for a technical application of manganese oxides in devices like artificial leaves or electrolysers and here further parameters gain key importance. As the following sections will show, the preparation route for the electrodes, the choice of the conductive substrate as well as the conductivity of the MnO_x catalyst itself also seem to play important roles for electrochemical WOC, making the identification of the "best MnO_x" even harder.

3 MnO_x based anodes for electrochemical water-oxidation catalysis

Manganese oxide based water oxidation electrocatalysis is known since the late 1970s, when ground-breaking studies were carried out in the groups of Tamura and Trassati. At first, electrodes were prepared via the thermal decomposition of a manganese nitrate solution drop-cast onto titanium foils [60]. The resulting anodes showed little WOC activity, which can be explained by the low electronic conductivity of the TiO_2 layer formed on top of the conductive backbone during the heating step. In a consecutive study, the disadvantage of using a self-passivating catalyst substrate was avoided by pressing MnO_2 into the form of a tablet to be used as an anode [36, 37]. Again, this electrode showed only little activity due to high ohmic losses. Furthermore, it was concluded from the variation (and mixing) of different MnO_x materials that the oxide composition and the average Mn oxidation state of the material employed as anode has a pronounced impact on the electrocatalytic performance and the stability. For electrodes mixed from Mn_2O_3- and MnO_2-powders, a higher dissolution during the anodic polarization was found compared to pure MnO_2 electrodes. Therefore, it was concluded that the anodic dissolution reactions proceed at Mn^{3+} sites. At this early phase, all electrochemical measurements were carried out either at highly acidic or strongly alkaline conditions. Interestingly, oxygen evolution could be observed in both regimes, but onset potentials were clearly lower in the alkaline, for which the onset of WOC was estimated at overpotentials of $\eta \sim 300$ mV.

Thus, these very early studies already showed that the electrode preparation method, the catalyst composition, the intrinsic electrical conductivity of the manganese oxide and also the employed electrolyte all affect the activities and stabilities of MnO_x electrocatalysts. In the following, we will address these factors

individually and present recent developments that have been made in each of them for the field of electrochemical water oxidation catalysis by MnO_x.

3.1 Variations of the electrode support material

The choice of the conductive substrate used as backbone for the MnO_x catalyst material greatly influences its WOC performance. In the case of MnO_x the application of solid MnO_x disks or rods prepared from powders is not feasible, because compared to other transition metal oxides commonly used for WOC, MnO_x generally show much higher electrical resistivities (Table 1). Therefore, it seems inevitable for MnO_x to avoid the transport of charge carriers through larger distances of the materials, which is most commonly achieved by applying just a thin layer of MnO_x catalyst on top of a much more conductive electrode support material. However, to find suitable support materials is far from straightforward, as they also have to fulfill a number of general requirements: (1) high electrical conductivity; (2) high chemical stability and (electrochemical) inertness up to at the high anodic potentials needed to drive the water oxidation reaction; (3) good stability even under the often drastic pH conditions of acidic or alkaline electrolysers; (4) a good thermal stability since MnO_x catalysts often require a sintering step at temperatures above 300 °C to establish good electrical contacts between the particles and the support; (5) a good availability and a low price; and (6) ideally a high surface area to increase the catalyst/electrolyte contact. In addition to this list, the experimentalist sometimes has to consider special requirements, such as transparency for UV/Vis light or X-rays in order to carry out spectroscopic

Tab. 1: Electrical resistivities of some metal oxide materials commonly used as anodes for electrochemical water-oxidation catalysis.

Metal-oxide	Electrical resistivity (Ω cm)[a]	Ref.
Mn_2O_3	0.2–8	[37, 61]
Mn_3O_4	$>10^6$	[62]
Na-birnessite	$5 * 10^5$	[63]
K-cryptomelane	$4 * 10^4$	[63]
RuO_2	$5 * 10^{-5}$	[64]
IrO_2	$6 * 10^{-6}$	[64]
NiO	$10^{-3} - 10^0$	[65]
Co_3O_4	10^0	[66]

[a]Please note that an exact quantitative comparison of the electrical resistivities of the different listed materials is at least questionable due to the different measurement techniques and sample preparations. Nevertheless, the values can be seen as a good approximation to estimate general conductivity trends.

studies. In the following we will present an overview of the most commonly used support materials for the electrochemical testing of MnO_x and mention possible advantages and disadvantages.

An electrochemical support material class that has very often been used in the context of WOC studies are transparent conductive oxides (TCOs). Typical examples are fluorine-doped/tin(IV)-alloyed indium(III) oxides (FTO/ITO), which are semiconducting oxide materials transparent to most visible light. Their n-type conductivity is either generated by oxygen vacancies, fluorine doping or by the substitution of the host metal by higher valency metal atoms (e.g. Sn in $Sn:In_2O_3$). For their use as conductive supports, thin layers of the TCOs are coated under high vacuum conditions onto glass substrates, resulting in glass slides with a thin conductive layer on top, which exhibit high degrees of transparencies for visible light. On their own, ITO and FTO can be considered to be WOC inactive both in NaOH and H_2SO_4 electrolytes (WOC onset potentials of +1.8 V and higher), making both materials suitable "innocent" substrates for the testing of water oxidation catalysts [67–69]. In comparison to ITO, FTO has a better chemical and thermal stability and lower price (making it the better choice for long-term experiments [70]), but both materials have often been used as substrates for WOC experiments [49, 71–83].

A further advantage of ITO or FTO substrates is their already mentioned transparency. As an example, one of our groups electrodeposited manganese oxides on ITO via different electrochemical coating protocols and monitored the changes of the Mn oxidation state of the deposited material by UV/Vis-spectroscopy [49, 75]. It was found that higher absorptions at 450 nm indicated a higher average oxidation state of the Mn ions and that during the pseudocapacitive charging of the electrode at potentials below the WOC onset, oxidation equivalents are accumulated due to $Mn^{II} \longrightarrow Mn^{III}$ and $Mn^{III} \longrightarrow Mn^{IV}$ transitions. In another, very influential work by the group of Nakamura [75], manganese oxide nanoparticles from the birnessite family were deposited on a FTO electrode to monitor the spectral changes during WOC at pH regimes ranging from 4 to 13. The recorded spectral changes at around 500 nm during the evolution of oxygen were explained by the accumulation of Mn^{3+} ions (from the oxidation of Mn^{2+}-ions) at the electrode surface, which were identified as key elements of the electrochemical reaction. This work also represented a first *in situ* spectroscopic detection of intermediates during WOC by manganese oxides. Generally, an increase of the average oxidation state of the bulk of different MnO_x polymorphs during operation is likely occurring, as seen by post operando soft- and hard- X-ray absorption (XAS)-measurements [49, 84, 85]. A discussion about the relationship between the XAS absorption changes and parameters like the Mn oxide conductivity can be found in a recent publication by some of us [84].

In addition to the transparency advantage there are further benefits of using TCO materials: (1) a good thermal stability up to 800 °C in air [71, 72, 74, 75, 77, 80, 83], which allows sintering and the synthesis of crystalline MnO_x phases at high temperatures [61, 79]; (2) easy characterization of the catalyst layer by TEM [75, 79, 82]; (3) the possibility to determine the band gaps of the MnO_x materials using UV/Vis spectroscopy [78]. A major disadvantage of using TCO materials are the quite low electrical sheet conductivity of the conductive layers ranging from 0.10 to 0.25 S/□ [86]. This resistivity becomes a substantial factor at high current densities or large electrode areas, thus making the use of FTO or ITO as support material for industrial WOC applications unlikely [87]. Additionally, there are no convincing ways to "activate" FTO or ITO surfaces for the deposition of MnO_x layers and hence it is not uncommon that the contact between the catalyst and the conductive oxide is mechanically weak, leading to the partial or complete detachment of the catalyst film under WOC conditions. Overall, MnO_x/TCO-anodes have clear advantages for fundamental investigations like mechanistic studies but will most likely not be suitable for the construction of even medium sized devices.

Another conductive electrode support material class is elemental carbon, used in electrochemistry since the early 19th century when Sir Humphrey Davy first used graphite electrodes for the production of alkaline metals. Since then, many different carbon materials have been developed for various electrochemical applications [88], including the role of support material for manganese oxide in WOC, for which they possess a number of profound advantages: (1) very good availability and (often) a low prize; (2) good chemical and electrochemical stability; (3) good thermal stability (up to 450 °C in air and up to 3000 °C in Ar); (4) high electrical conductivity (e.g. 2–3 10^5 S m^{-1} $\parallel$ to the basal plane and 3 10^2 S m^{-1} $\perp$ to the basal plane of graphite) [89]; (5) high intrinsic surface areas for materials like carbon nanotubes (CNTs) or carbon fibers; (6) the possibility to modify the material surface for example by the introduction of oxygen functionalities in order to enhance the electric and mechanical contact between MnO_x and C; [90–92] (7) suitability for some spectroscopic techniques, e.g. vibrational or X-ray spectroscopies (XAS, XPS) [93, 94].

Some of the most commonly used carbon-based electrode materials are graphite rods or sheets, CNTs, carbon fibers (in the form of papers or felts), amorphous carbon (carbon blacks), graphene, highly oriented pyrolytic carbon (HOPG) and – most popular for electrochemical analysis – glassy carbon (GC). This material was discovered in 1962 and consists of randomly intertwined ribbons of graphitic planes prepared by heating different organic polymers under pressure in an inert gas atmosphere at 1000–3000 °C [88, 95, 96]. GC exhibits a high (electro)chemical stability, is commercially available and can be manufactured into many shapes such as rotating disk electrodes which have

often been used as substrates for the characterization of MnO_x at WOC conditions [92, 97, 98]. On the other hand, GC has only a small intrinsic surface area (similar to the TCO supports described above). Some research groups increased the contact area between the catalyst and the electrolyte by first depositing MnO_x catalysts on CNTs and then coating GC disks with the obtained MnO_x/CNT hybrids [92, 98, 99]. Another possibility to increase the intrinsic surface areas is to use an electrode material that is based on carbon fibers, e.g. carbon fiber paper (CFP) or carbon felts (CF), which are well-known in electrocatalysis e.g. as gas diffusion layers (GDL) in polymer electrolyte (PEM) fuel cells or electrolysers [100, 101]. Furthermore, CFPs and CFs have also been used as catalyst supports in so called gas diffusion electrodes (GDE) [102, 103].

Despite these many advantages, there are also some drawbacks of carbon materials like the possible vulnerability to corrosion. From a thermodynamic point of view, carbon is only stable within a small potential window in water, as for example the four-electron oxidation of C to CO_2 could occur already at potentials of $E > 200$ mV [104], and thus far below the thermodynamic potential of water oxidation. Fortunately, this reaction is kinetically severely hindered due to the complex sequence of reaction steps leading from graphite to CO_2, which is known to proceed via the formation of surface oxides at defect sites of the carbon material [105–108]. One of our groups found that the number of such defect sites correlates directly with the degree of graphitization (quantified using Raman spectroscopy) and that graphitic carbon materials are therefore best chosen as MnO_x supports in order to obtain stable anodes for water oxidation [109]. Using in-operando membrane inlet-mass spectrometry (MIMS) to detect CO_2 as likely corrosion product, we observed that only graphitic carbon materials are sufficiently stable in water at the potentials needed for WOC by MnO_x (e.g. $E \geq 1.75$ V at pH 7.0). On the other hand, low graphitized carbons suffered from corrosion, leading to a loss of contact between MnO_x and C (and thus a deactivation of such anodes) over time. On the other hand, it has been reported that highly graphitic substrates like GC or HOPG, the latter a highly pure and very ordered form of graphitic carbon, can be used with little corrosion problems even at potentials above 2 V [67]. However, a disadvantage of GC or HOPG are their low surface areas, so that additional modifications are usually needed to reach interesting WOC current densities (see above).

In summary, this short introduction on TCOs and carbon materials as possible conductive substrates for manganese oxides has illustrated that choosing the right material for this task can be quite challenging. For analytical studies where a flat, UV/Vis transparent support is important, TCO materials are for sure a good choice. On the other hand, nanostructured, graphitic carbon materials like CFP appear to be especially well suited as backbones for MnO_x catalysts if devices like

electrolysers are the target of a study. Of course, many other types of conductive supports like gold, stainless steel, platinum or nickel foam have been used in this context as well [74, 85, 94, 110, 111], but none of them seems to have substantial advantages over TCOs or C to us, so that a detailed discussion of these substrate materials is omitted here.

3.2 Routes for electrode preparation

There are many ways to deposit manganese oxides on conductive electrode backbones with the aim to prepare anodes for electrochemical water oxidation (see Figure 3), such as e.g. electrodeposition [49, 61, 71, 72, 74, 78, 79, 81, 82, 85, 93, 94, 97, 110, 114–117], dip-coating [118], drop-casting [92, 98, 99, 119, 120], spin-coating [121], spray-coating [75–77, 80], screen-printing [73, 77, 118], direct redox-deposition [98, 109], calcination of surfaces impregnated by manganese

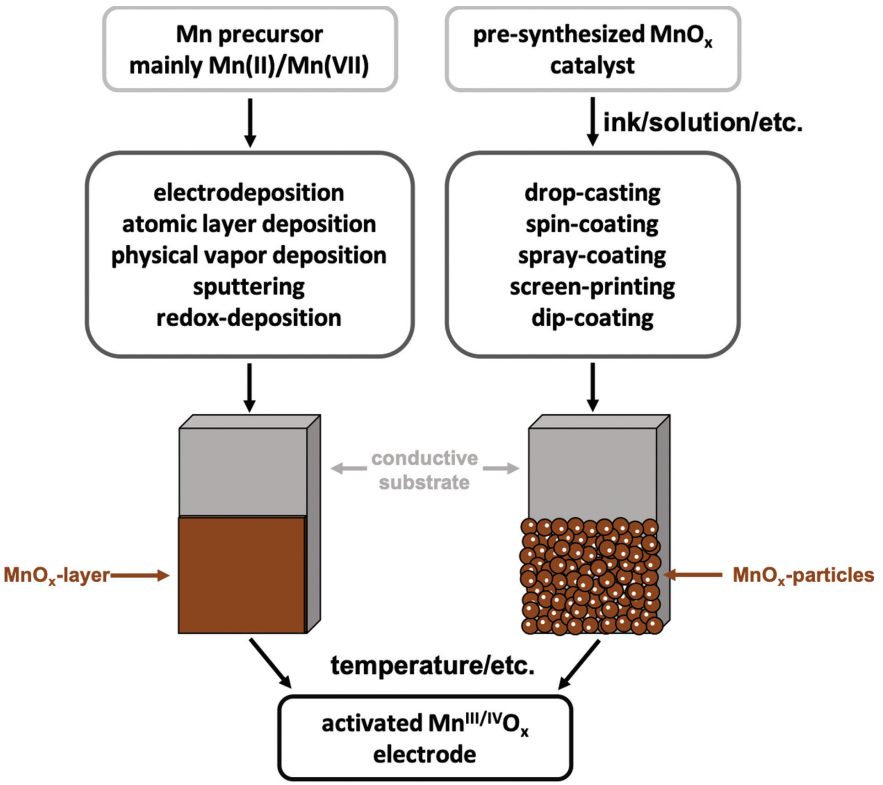

Fig. 3: Schematic representation of different preparation techniques for MnO_x-based electrodes for the OER.

salts [37, 75], atomic layer deposition [122–125], physical vapor deposition [126] or reactive sputtering (DC or AC sputtering) [127, 128].

As indicated by the large number of references cited above, the electrodeposition of manganese oxides has so far been the most widely used technique. Electrodeposition has the big advantage that the thickness and composition of the catalyst layer can be tuned by the deposition protocol. Furthermore, various post-deposition treatments even allow access to different MnO_x phases. As a result, there are nearly as many different electrodeposition protocols as publications. However, most of them have the following basic parameters in common: (1) the Mn oxides are deposited anodically, starting from an aqueous solution containing Mn^{2+} and acetate, nitrate, sulfate or chloride as counterions; (2) to increase the ionic conductivity of the electrolyte and in order to control the pH, additional ionic compounds like $MgSO_4$, Na_2SO_4, $(Na/K)NO_3$, NaCl, $NaClO_4$, acetate/borate buffer, etc. are often added. These additives are known to influence both the composition and the structure of the electrodeposited MnO_x, which in turn both have an effect on WOC activity and stability. However, systematic investigations on this topic are so far missing; (3) depositions are carried out at moderate pH values ranging from around pH 5.5 [61, 72, 78, 79] to pH 9.2 [94].

Even as these parameters already allow for substantial variations, the factor having the biggest influence on composition, structure and activity/stability of the MnO_x electrocatalyst is the electrochemical protocol. There are several ways to achieve the deposition of MnO_x, e.g. voltage cycling in the anodic potential range [49, 81, 82, 93, 97], constant anodic potentials high enough to oxidize Mn^{2+} or the application of a constant deposition current density (and thus deposition potentials which in some cases increase over time) [49, 61, 71, 72, 74, 78, 79, 82, 94, 114]. One of our groups studied the influence of the electrochemical protocol on the activity of the deposited manganese oxide in detail and found that a higher activity can be achieved if the catalyst is deposited via a voltage cycling protocol compared to one using a constant potential [49]. Several reasons for this behavior have been proposed: (1) the more active MnO_x obtained from the cycling protocol showed a lower average oxidation state of Mn $\sim$+3.8 when exposed to oxidizing potentials compared to Mn $\sim$+4.0 in the film deposited at constant potential; (2) in both cases, a layered, birnessite-type manganese oxide is formed, but its structure is significantly less ordered in the case of the cycling protocol. These results on oxidation states and structures were later confirmed in a study by Huynh et al., which additionally showed that a process where a further cathodic pulse is applied to the anodically deposited catalyst film leads to an even more active MnO_x catalyst [82, 129].

Despite the possible advantages of MnO_x electrodeposition at strongly varied electrochemical conditions, catalysts formed at constant potential or current

density conditions are much more common and also reach high electrocatalytic activities. However, here the as-deposited manganese oxide films usually have to be activated further in a heat-treatment step to reach the best WOC results [61, 74, 78, 79, 94, 114, 130]. In work by another of our groups, an amorphous (most likely layered) manganese oxide film was first deposited at constant current density conditions and then annealed at 300 °C (in air), 500 °C (in air) or 600 °C (in argon), resulting in the formation of activated amorphous MnO_x, Mn_2O_3 or Mn_3O_4, respectively [78, 79]. In electrocatalysis experiments, the activated amorphous MnO_x- and the Mn_2O_3-materials showed the smallest onset potentials and highest catalytic currents.

Based on the results presented so far, one can conclude that electrodeposition protocols starting from aqueous Mn^{2+} solutions generally lead to the formation of amorphous, birnessite-type manganese oxides. These as-deposited materials can already be quite active in WOC (e.g. when prepared via a voltage cycling protocol) and can often be activated further by subsequent heat-treatment or cathodization steps.

Another common route to immobilize MnO_x on conductive supports is to pre-synthesize the desired oxide phases as powders and then use drop-casting [92, 99, 119], spin-coating [121], spray-coating [75–77, 80] or screen-printing [73, 77, 118] methods to coat the chosen support. These procedures have in common that at first suspensions ("inks") of the MnO_x have to be prepared prior to the deposition and these often contain additives like polyethylene oxide (PEO) [77], polytetrafluoroethylene (PTFE) [73], Nafion [98, 99], ethyl cellulose [73] or ethylene glycol [118] in order to obtain stable coatings. A major advantage of this overall strategy is that well characterized, pre-synthesized catalyst materials are used, for which it is often possible to control material properties like composition, oxide phase or morphology quite well. Thus, one can evaluate the influence of these parameters on the materials' activities and stabilities under WOC conditions much better [119] and even carry out mechanistic studies, where a well characterized catalysts material is essential.

Screen-printing is a standard technique in electronics and it has also been used to prepare anodes for WOC [73, 77]. The procedure requires an ink containing polymeric binders which are evaporated or decomposed after printing in a sintering step. As a consequence of this, highly porous metal oxide coatings are often obtained, for which the thickness and the coated area can be controlled very well. In a study where a pre-synthesized Ca-birnessite was screen-printed onto FTO supports, one of our groups investigated the influence of parameters like oxide film thickness, binder type or sintering temperature on electrochemical water-oxidation activity and stability in a neutral phosphate electrolyte. It was found that a 30 min. annealing step at 450 °C is essential to remove the organic

compounds of the ink and to obtain a mechanically stable catalyst coating. As might have been expected, the choice of organic binder also greatly affects the catalyst's performance and here the best results were recorded for anodes prepared from PEO-containing inks. Subsequently, the relation between the layer thickness and the catalytic activity was investigated revealing a maximal current density for 10 μm thick oxide coatings. Catalyst layers thinner or a thicker than this value showed lower WOC current densities, a result that was interpreted as a hint that it is necessary to find a compromise between the lower electrical resistivity of thinner coatings and the increased number of active sites in thicker ones [93].

Spray-coating, known for the fabrication of large area thin films in the electronics industry, is another versatile and promising method for the preparation of manganese oxide electrodes. The group of Nakamura established a spray-coating process in which a dilute MnO_x colloid is first formed by the reduction of $KMnO_4$ by $Na_2S_2O_3$ in water. This solution was then repeatedly (up to 600 times) sprayed onto FTO serving as conductive substrate and afterwards calcinated at 500 °C to form a stable coating of δ-MnO_2. Alternatively it has been reported that stable and easily scalable MnO_x coatings can also be prepared by a layer by layer deposition of a manganese acetate solution on a conductive substrate (FTO) using an air-spray gun [83]. Subsequent annealing of this deposited precursor for 2 h at 500 °C in an O_2 atmosphere leads to the formation of a smooth and robust oxide film which was identified to be crystalline Mn_2O_3. The authors underline that the high reproducibility, the precise control of the film thickness, the high production speed and the simple scalability are all important advantages of this coating process. Electrodes of this type needed an overpotential $\eta = 400$ mV to reach a current density $j = 10$ mA cm^{-1} in 1 M KOH.

Drop-casting has also been used as a rather simple route to coat conductive substrates by MnO_x [92, 98, 99, 120]. This process starts with dropping the catalyst containing solution onto the support followed by the spontaneous evaporation of the low boiling solvent. A high-temperature sintering step is omitted, so that conductive additives like Nafion are commonly added to the drop-casting solution in this process to yield mechanically stable and electronically well-connected catalyst coatings. As the method is carried out at mild conditions and it is especially easy to control the amount of catalyst loaded onto the conductive substrate, drop-casting has been regularly used to screen catalyst libraries or to study loading effects. Another advantage of the gentle coating procedure is its suitability to attach MnO_x materials to rotating-disc electrodes (RDEs), which one cannot heat to high temperatures [98, 99].

As an alternative to adding conductive polymers like Nafion, it is also quite common to use carbon powders like Vulcan XC-72 [120] or charcoal [119] to

enhance the electric contact between MnO_x catalysts and support. An elegant way to extend this approach to nanostructured carbon materials of increased electrochemical active surface area was developed by Mette et al. [99] and further improved by Bergmann et al. [92]. The groups studied MnO_x which was deposited onto the surface of functionalized carbon nanotubes (fCNTs) either by (a) impregnation of the CNTs with Mn^{2+} followed by permanganate treatment or (b) impregnation with Mn^{2+} followed by a calcination step at 300 °C in air. Both techniques are cheap, well established, scalable and typically lead to the deposition of thin layers of the active materials. The MnO_x formed via route (a) was identified as an amorphous layered manganese oxide with an average oxidation state of +3.5, the one from route (b) as a mixture of β-MnO_2 and γ-MnO_2 with an oxidation state around +3.0. Both composites were attached via drop-casting onto GC-RDEs, where better WOC activities and stabilities at pH 7.0 were observed for the β-/γ-MnO_2/CNT system.

Motivated by these very promising first reports on MnO_x/C-anodes (see Figure 4) for water-oxidation, some of us developed an alternative way to prepare such hybrids, this time without the need to use binders or additives [109, 131]. Here, the carbon material does not only serve as conductive and mechanical backbone, but also as reducing agent for MnO_4^- to deposit MnO_x directly onto the surfaces of carbon materials (Figure 4). After a sintering step in air at 400 °C, the binder-free MnO_x coating was again identified as amorphous, potassium containing birnessite with an average oxidation state of +3.7. Loading optimized

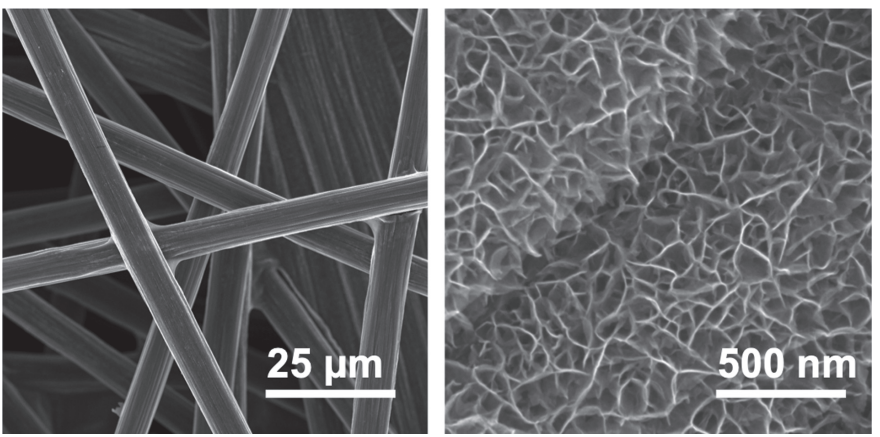

Fig. 4: High surface area graphitized carbon fiber paper (CFP, Toray TGP-H-60) before (left) and after (right) the decoration with MnO_x via direct redox deposition from an acidic permanganate solution.

MnO_x/C-electrodes of this type showed promising electrocatalytic activities and stabilities when operated under neutral conditions. This method is cheap, easily scalable and applicable to many different carbon support materials, as e.g. shown by Antoni et al. who used fCNTs as carbon source [98].

As a final preparation route we would like to mention low-pressure methods like atomic layer deposition (ALD) [122, 123, 125, 132], physical or chemical vapour deposition (PVD/CVD) or sputtering [124, 126, 127]. All four techniques are technologically much more demanding than the previous methods, but allow the benefit of depositing catalytic MnO_x films in highly controlled ways. ALD can be used to prepare pin hole free monolayer to multilayer coatings with full control over the catalyst thickness on many substrates. The group of Pickrahn et al. deposited a 40 nm thin, planar MnO layer onto a glassy carbon substrate by using $[Mn(EtCp)_2]$ as volatile manganese precursor and water as co-reactant [122, 132]. Subsequent annealing of the coating at 480 °C led to the formation of a very rough and porous Mn_2O_3 coating. Both MnO_x phases are active in electrochemical water-oxidation and exhibit nearly identical activities, most likely due to similar surface structures induced by the oxidative potentials applied at WOC conditions. Furthermore, the team was able to show that the application of their "ALD-MnO_x" on high surface area GC (HAS-GC), which has a much higher surface area, leads to an enhanced geometric activity indicating that the catalytic activity scales with the surface area. However, ALD is a very slow and expensive deposition technique and hence the MnO_x layers that are accessible in a reasonable time are only a few nanometers thick. Further possible disadvantages are corrosion and mechanical detachment, which are well known to occur for very thin MnO_x films [49]. However, both mentioned studies on ALD-MnO_x do not provide any long-term measurements.

In contrast to ALD, physical vapour deposition offers much faster deposition rates and thus the option to prepare thicker and probably more durable catalyst films in a reasonable time. PVD can also be used to deposit films with different morphologies and compositions. Therefore, metal oxide layers with well-defined nano-architectures are accessible. Together with the Mohney group one of our teams deposited layers of elemental manganese with varying thicknesses on conductive ITO substrates by electron beam evaporation [126]. Subsequent oxidation of Mn in air for 16 h at 300 °C yielded very smooth, brown MnO_x-layers which were characterized as mixtures of MnO and Mn_3O_4 with thicknesses ranging from about 100–400 nm. The films only exhibited small catalytic currents due to their low surface areas, but as the long-term stabilities of these "PVD-MnO_x" anodes proved to be very good, they mark a good starting point for further improvements and optimizations (as e.g. already achieved by the introduction of Ca^{2+}-ions into such films via a co-sputtering process) [127].

The deposition of thin manganese oxide films can also be achieved by reactive magnetron sputtering, a simple and efficient technique to prepare homogeneous, compact layers of materials on various supports (see Figure 5). In dependence of the substrate temperature, different Mn-oxides can be obtained: at RT, an amorphous MnO_x is formed, which changes its structure with increasing temperature to nano-crystalline γ-MnO_2 and at ~350 °C transforms again into α-Mn_2O_3. Both the γ-MnO_2 and the α-Mn_2O_3 films showed similar catalytic OER activities with overvoltages of ~380 mV for 10 mA cm^{-2} under alkaline conditions (pH 13.8) [112, 113].

In summary, there is a plethora of different possibilities to deposit manganese oxides on conductive materials. In combination with the large number of possible substrates this leads to nearly endless possibilities for the preparation of MnO_x-functionalized electrodes. Even as different MnO_x/substrate combination types clearly show varying catalytic activities and stabilities, it is currently not possible to identify a clear winner among the electrode preparation techniques, e.g. as it appears that every MnO_x/substrate pair has be optimized individually. However, as a general trend, MnO_x materials of low order deposited on conductive, nanostructured backbones of high surface areas are often very good candidates for well-performing manganese oxide-based water oxidation anodes.

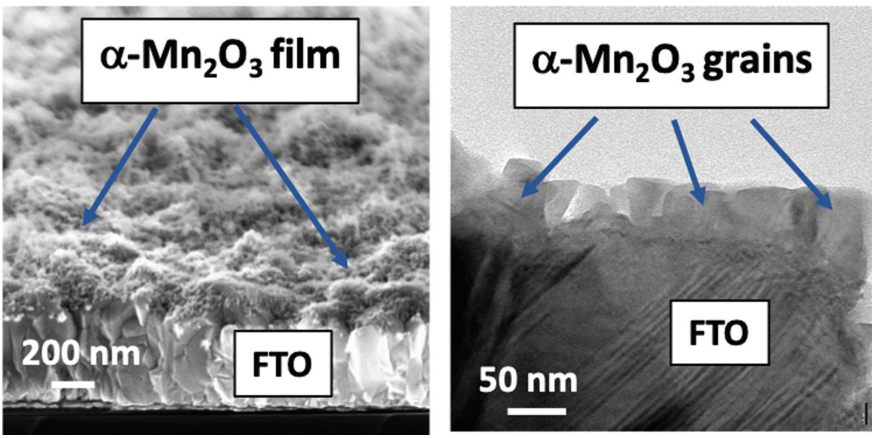

Fig. 5: SEM (left) and TEM (right) images of a α-Mn_2O_3 layer deposited at 350 °C on TCO glass (F:SnO_2, FTO) by reactive magnetron sputtering. The layer homogeneously covers the FTO substrate. The Mn_2O_3 crystallites grown on top of the FTO substrate have a size of about 50 nm. The tooth-like morphology indicates a growth of facetted nanocrystals [112, 113].

3.3 Electrolyte variations and influences of the pH

In electrochemical water oxidation it is well known that the choice of the electrolyte has an enormous impact on the catalytic activity and stability of the metal oxide catalyst [133, 134]. To benefit from the very good conductivity of concentrated acids or bases, water oxidation electrocatalysis has commonly been studied for either very acidic or very alkaline conditions. Also some of the very early studies on WOC by MnO_x were conducted either in 1 M H_2SO_4 or 1 M KOH [37, 60] and significant differences between the performances at pH ~0 and pH ~14 were already found, but a reason for this phenomenon could not be given. Later, WOC by MnO_x was additionally studied in detail for less harsh, near neutral electrolytes, as it became clear that especially photoelectrochemical systems like artificial leaves demand conditions where the photoabsorber and/or junction materials are stable as well [103, 135]. For example, silicon is easily passivated (forming SiO_2) under alkaline conditions and corrodes in acid. As a result, many reports on the catalytic activity of manganese oxides operated close to pH 7 are available, where the influence of factors like the addition of buffering bases or the electrolyte concentration on the stability and activity of the MnO_x have been addressed.

As can be seen in the Pourbaix diagram for manganese, MnO_x show a good stability over a large pH range. They generally suffer less from corrosion under neutral to acidic conditions while this is a problem e.g. for NiO_x- or CoO_x-based electrodes [136–138]. As an example, Nocera and co-workers extensively investigated the electrocatalytic activity of electrodeposited MnO_x/FTO anodes in phosphate buffers of three different pH values (pH 2.2/7.0/12.2) [81]. The ionic strengths of the solutions were adjusted by adding KNO_3 in order to exclude pure conductivity effects. First, the influence of the buffer base concentration on the catalytic activity for the three pH values was tested resulting in a zero-order dependence of the activity on the phosphate ion concentration under all selected pH values. On the first view, this result indicates that the buffer base is not involved in the rate determining step of the mechanism for water oxidation at MnO_x, so that the activity of the catalyst cannot be increased by adding proton accepting ions. However, the reaction rate determination was carried out at relatively low current densities where the proton uptake by water molecules could be sufficient. Recently it was shown by some of us that the OER current for amorphous cobalt oxide catalysts at neutral pH strongly depend on the rate of the proton transfer to available bases [134]. This points to the fact, that especially at higher current densities (which are needed for a possible industrial applications) mass-transport limitations come into play and the availability of high concentrations of a proton accepting base would thus enhance OER activity. The aforementioned study also investigated

the influence of the pH on the activity and the mechanism [81]. Kinetic analysis revealed two competing mechanisms under acidic and alkaline conditions and a competition between both at neutral pH. Higher activities were found for electrodes operated in alkaline pH, which was explained by the higher stability of Mn^{3+} ions at the oxide surface for pHs above 9.

In 2012, Nakamura and co-workers investigated the behavior of MnO_x electrodes under different pH conditions, but here with a special focus on changes of the MnO_x catalyst material during operation detected by *in situ* spectroelectrochemistry [75]. For pH >9, a non-Nernstian decrease of the onset potential was observed, leading to significantly lower overpotentials in alkaline media. These results were accompanied by a change in the optical absorption spectrum which the authors again assigned to an increase of the number of Mn^{3+} ions available as active sites for catalysis. At intermediate to acidic pH conditions, such Mn^{3+} sites are removed by the disproportionation into Mn^{2+} and Mn^{4+}, so that Mn^{2+} has to be re-oxidised to Mn^{3+} prior to the catalysis. This study can be seen as a starting point for further work aiming to stabilize the active Mn^{3+} form under WOC conditions. As an example, the Nakamura group later modified spray-coated δ-MnO_2/FTO electrodes with an amine containing polymer (poly(allylamine) hydro-chloride, PAH) [76]. It is known that Mn–N bonds can stabilize Mn^{3+} against disproportionation and indeed a lower onset potential for the evolution of O_2 at pH 8 was detected.

The Nakamura group also investigated the influence of the addition of proton accepting bases on electrochemical WOC under neutral conditions [80]. It was found that the addition of 0.5 M pyridine to a 0.5 M Na_2SO_4-solution led to a large decrease of the onset potential by around 200 mV. As a control, pyridine was also added to a Na_2SO_4-electrolyte at pH 4 (where ~95% of the pyridine molecules are protonated). Here, no enhancement of the catalytic activity was observed, indicating that the proton-accepting base is responsible for the activity gain and that a proton coupled electron transfer step might be involved in the rate-determining reaction step at neutral conditions. In the following, five pyridine derivatives with pK_a values ranging from ~5 to 7.5 were evaluated as potential bases for WOC at pH 7.5. The best results were found for γ-collidine, which had the highest pK_a-value of the series ($pK_a = 7.48$), making it the best proton acceptor at these conditions and resulting in an impressive 15-fold higher O_2-evolution rate compared to WOC in the absence of bases. Although the studies of the Nakamura group clearly demonstrated that water-oxidation activity can be greatly enhanced by the addition of suitable bases, it is worth to mention that pyridines can be oxidized themselves at WOC conditions so that pyridine-containing electrolytes are not the best choice for this task [80].

Inspired by these reports, some of us tested the influence of five different 0.1 M electrolyte systems in the pH-range between ~5 and 9 on the electrocatalytic performance of screen-printed Ca-birnessite/FTO electrodes [139]. We found that an operation in phosphate buffer at pH 7 resulted in the best activity and stability within the series (see Figure 6) and found several possible reasons to explain this trend: (1) the phosphate buffer exhibits a higher proton affinity than e.g. acetate or (even more so) sulfate [134]; (2) the 0.1 M phosphate buffer solution exhibited the highest ionic conductivity of all tested systems; (3) methyl phosphonate showed an oxidation event at around +1.8 V meaning that it is not completely redox stable. After identifying phosphate as the preferred buffer system, the dependence of the WOC current density on the phosphate buffer concentration were investigated using chronopotentiometry for $j = 1$ mA cm^{-2} and pH 7. It was found that it was possible to further lower the necessary overpotential by around 100 mV when the phosphate buffer concentration was increased from 0.1 to 0.5 M (see Figure 6). This result is contradicting the observations of the Nocera group for low current densities [81], but is in line with the findings of the teams of Nakamura and Dau [80, 134] and confirms the importance of a suitable base especially at higher current densities where mass-transport becomes the rate limiting factor.

It can be concluded, that phosphate buffers are especially well-suited electrolytes for water oxidation by manganese oxides under neutral conditions which

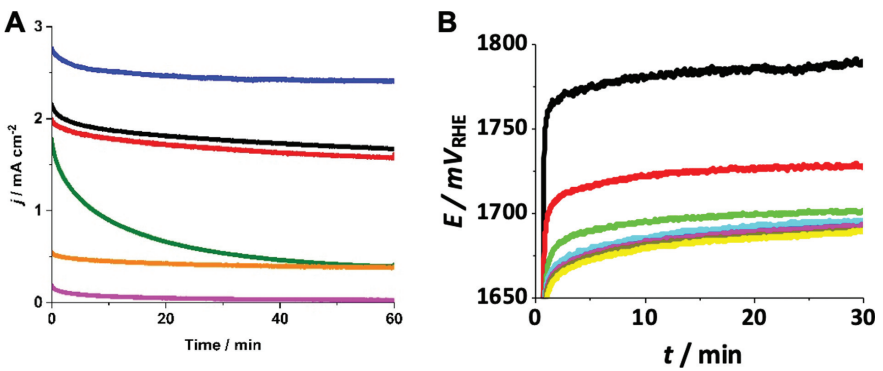

Fig. 6: (a) Chronoamperometry traces for Ca-birnessite/FTO electrodes immersed in 0.1 M phosphate buffer (pH 7, blue trace), 0.1 M borate buffer (pH 9.2, black trace), 0.1 M methyl phosphonate (pH 7, red trace), 0.1 M imidazolium buffer (pH 7.4, green trace), 0.1 M acetate buffer (pH 4.8, orange trace) and 0.1 M potassium sulfate (pH 7.0, pink trace). In all cases a constant potential of +1.71 V vs. RHE ($\eta = 480$ mV) was applied. (b) Chronopotentiometry experiments conducted at a constant current density of $j = 1$ mA cm^{-2}, the concentration of the phosphate buffer electrolyte has been varied as follows: black – 0.033 M, red – 0.1 M, green – 0.2 M, blue – 0.3 M, cyan – 0.4 M, purple – 0.5 M, yellow – 0.6 M, brown – 0.7 M [139].

explains why they have been the first choice by many different groups for WOC at pH ~7 [49, 71, 74, 77, 78, 81, 82, 92–94, 109, 114, 116, 121, 126, 128, 140]. The main advantages of this buffer system are: (1) good availability and affordable price; (2) good redox stability over a wide potential range; (3) due to the three acid constants of phosphoric acid ($pK_{a1} = 2.1$; $pK_{a2} = 7.2$; $pK_{a3} = 12.4$), it can be used over nearly the entire pH range; (4) the high solubility in water allows for making phosphate buffers with high concentrations and high ionic conductivities.

In addition to the development of MnO_x catalysts for water electrolysis under neutral pH, highly alkaline conditions (for example 1 M KOH or NaOH) have been extensively studied as well [61, 72, 73, 83, 97–99, 110, 119, 120, 122, 124, 128, 132]. These electrolytes also show numerous advantages like (1) high solubility leading to the possibility of reaching very high ionic conductivities; (2) no redox stability issue as OH^- is derived from the water; and (3) very high reactivity with protons. As a result, WOC by MnO_x generally proceeds at higher rates in highly alkaline electrolytes compared to pH ~7 and the best MnO_x electrodes reach the benchmark current density of $j = 10$ mA cm^{-2} already at overpotentials $\eta = 350$ mV when operated in 1 M KOH (α-Mn_2O_3/FTO [78] and $K_{0.1}MnO_x$/CFP, see also Table 2). Additionally, higher stabilities have been reported for electrodes operated under these conditions [75, 77, 81, 131, 142]. In a study by two of our groups, the long-term stabilities of MnO_x anodes was tested at pH 2.5/7.0/12.0. There, significantly higher stabilities were observed for electrodes operated at pH 12.0, explained by a suppressed formation of permanganate which was found to be higher for electrodes operated at pH 7.0 and 2.5 [131]. However, the remarkable activity gains found for $NiFeO_x$ when operated in alkaline electrolysers are not matched by MnO_x, so that very alkaline electrolytes do not seem to be the particular strength of MnO_x used for WOC.

For the acidic regime, Lewis and co-workers tested the WOC activity of a $NiMnSbO_x$ prepared by sputter deposition in 1 M H_2SO_4 [138]. Although the best catalyst needed a rather high overpotential of $\eta = 730$ mV to reach a current density of 10 mA cm^{-2}, a remarkable long-term stability (>1 week) was found. Li et al. confirmed this observation for a carbon fiber paper substrate coated by MnO_x, which could be operated in a PEM-electrolyser setup (H_2SO_4, pH ~2) at a current density of 10 mA cm^{-2} ($E = 1.73$ V) for more than 8000 h (!) without a clear decrease of the activity [141]. Furthermore, the group determined the potential window where MnO_x can be operated at pH 2 to lie between +1.4 and 1.75 V. At lower or higher potentials, UV/Vis spectroelectrochemical measurements indicated the formation of Mn^{2+} or MnO_4^-, respectively.

In summary, the choice of the right proton accepting, redox innocent electrolyte system for manganese oxide based water-oxidation is both important and challenging. Under near neutral conditions, an optimization of the electrolyte is

Tab. 2: Summary of the electrocatalytic performance of different manganese oxide electrodes developed for the OER.

#	MnO_x cat. phase	Cat. mass/thickness	Dep. method	Substrate	Electrolyte pH	Performance	Stability	Ref.
1	MnO	40 nm	ALD	GC	0.1 M KOH 13	~610 mV @ 10 $\frac{mA}{cm^2}$ [a]	No data provided	[122]
2	MnO	40 nm	ALD	HSA-GC	0.1 M KOH 13	~490 mV @ 10 $\frac{mA}{cm^2}$ [a]	No data provided	[132]
3	MnO	300 nm	Spin-coating	FTO	0.5 M KPi 7	~550 mV @ 5 $\frac{mA}{cm^2}$ [a]	No data provided	[121]
4	Mn_3O_4	650 nm	ED + 600 °C	FTO	1 M KPi 7	~570 mV @ 1 $\frac{mA}{cm^2}$ [a]	0.4 $\frac{mA}{cm^2}$ @ 470 mV, 1 h[d]	[79]
5	α-Mn_2O_3	40 nm	ED + 480 °C	GC	0.1 M KOH 13	~540 mV @ 10 $\frac{mA}{cm^2}$ [b]	No data provided	[97]
6	α-Mn_2O_3	40 nm	ALD + 480 °C	GC	0.1 M KOH 13	~580 mV @ 10 $\frac{mA}{cm^2}$ [a]	No data provided	[122]
7	α-Mn_2O_3	650 nm	ED + 500 °C	FTO	1 M KPi 7	~340 mV @ 1 $\frac{mA}{cm^2}$ [a]	0.6 $\frac{mA}{cm^2}$ @ 470 mV no degradation after 1 h operation time[d]	[79]
8	α-Mn_2O_3	400 nm 190 $\frac{mg}{cm^2}$	ED + 500 °C	FTO	1 M KOH 14	~340 V @ 10 $\frac{mA}{cm^2}$ [a]	10 $\frac{mA}{cm^2}$ @ 400 mV, no degradation after 2 h operation time[e]	[61]
9	α-Mn_2O_3	40 nm 20 $\frac{mg}{cm^2}$	ED + 500 °C	FTO	1 M KOH 14	~400 mV @ 10 $\frac{mA}{cm^2}$ [a]	10 $\frac{mA}{cm^2}$ @ 500 mV, no degradation after 2 h operation time[e]	[61]

Tab. 2 (continued)

#	MnO_x cat. phase	Cat. mass/thickness	Dep. method	Substrate	Electrolyte pH	Performance	Stability	Ref.
10	α-Mn_2O_3	1 mm 810 $\frac{mg}{cm^2}$	Spray-coating + 500 °C	FTO	1 M KOH 14	~400 mV @ 10 $\frac{mA}{cm^2}$ [a]	10 $\frac{mA}{cm^2}$ @ 530 mV, 60 h[e]	[83]
11	α-Mn_2O_3	200 nm	ED + 550 °C	FTO	0.1 M KPi 7	~630 mV @ 6 $\frac{mA}{cm^2}$ [a]	1.1 $\frac{mA}{cm^2}$ @ 470 mV, 12 h[d]	[71]
12	α-MnO_2	204 $\frac{mg}{cm^2}$	Drop-casting	pyrolytic graphite	0.1 M KOH 13	~490 mV @ $\frac{mA}{cm^2}$ [b]	5 $\frac{mA}{cm^2}$ @ 600 mV, instable after 3 h[d]	[120]
13	β-MnO_2	1.4 μm	Screen-printing + 450 °C	FTO	0.1 M NaOH 13	~740 mV @ 10 $\frac{mA}{cm^2}$ [a]	No data provided	[73]
14	β-MnO_2	4.3 mm	Screen-printing + 450 °C	FTO	0.1 M NaOH 13	~550 mV @ 10 $\frac{mA}{cm^2}$ [a]	14 $\frac{mA}{cm^2}$ @ 600 mV 1 h, 2 M KOH[d]	[73]
15	β-MnO_2	204 $\frac{mg}{cm^2}$	Drop-casting	pyrolytic graphite	0.1 M KOH 13	~600 mV @ 10 $\frac{mA}{cm^2}$ [b]	Instable @ 5 $\frac{mA}{cm^2}$ [d]	[120]
16	β-MnO_2 amorphous	650 nm	ED + 300 °C	FTO	1 M KPi 7	~440 mV @ 1 $\frac{mA}{cm^2}$	0.1 $\frac{mA}{cm^2}$ @ 470 mV, 1 h[d]	[79]
17	γ-MnO_2 amorphous	No data	Drop-casting + 220 °C	CFP	0.5 M Na_2SO_4 2	~500 mV @ 10 $\frac{mA}{cm^2}$ [a]	10 $\frac{mA}{cm^2}$ @ 500 mV, 8000 h[e]	[141]
18	δ-MnO_2	No data	ED + 90 °C	FTO	1 M NaOH 14	~520 mV @ 10 $\frac{mA}{cm^2}$ [a]	0.4 $\frac{mA}{cm^2}$ @ 440 mV, 15 h[d]	[72]
19	δ-MnO_2 /fCNT	No data	Drop-casting	GC	0.1 M KPi 7	~ 600 mV @ 10 $\frac{mA}{cm^2}$ [b]	No data provided	[99]
20	δ-MnO_2 ($Ca_{0.2}MnO_x$) amorphous	1.2 μm	Screen-printing + 450 °C	FTO	0.066 M KPi 7	~820 mV @ 1 $\frac{mA}{cm^2}$ [c]	No data provided	[77]

Tab. 2 (continued)

#	MnO_x cat. phase	Cat. mass/thickness	Dep. method	Substrate	Electrolyte pH	Performance	Stability	Ref.
21	δ-MnO_2 ($Ca_{0.2}MnO_x$) amorphous	9.6 μm	Screen-printing + 450 ° C	FTO	0.066 M KPi 7	~480 mV @ 1 $\frac{mA}{cm^2}$ [c]	1.0 $\frac{mA}{cm^2}$ @ 480 mV, 2 h [d]	[77]
22	δ-MnO_2	204 $\frac{mg}{cm^2}$	Drop-casting	pyrolytic graphite	0.1 M KOH 13	~740 mV @ 10 $\frac{mA}{cm^2}$ [b]	Instable @ 5 $\frac{mA}{cm^2}$ [d]	[120]
23	δ-MnO_2 amorphous	204 $\frac{mg}{cm^2}$	Drop-casting	pyrolytic graphite	0.1 M KOH 13	~590 mV @ 10 $\frac{mA}{cm^2}$ [b]	instable @ 5 $\frac{mA}{cm^2}$ [d]	[120]
24	δ-MnO_2 amorphous	<50 nm	ED + cathodization	FTO	0.1 M KPi 2.5	~600 mV @ 1 $\frac{mA}{cm^2}$ [c]	0.1 $\frac{mA}{cm^2}$ @ 500 mV, 8 h [e]	[82]
25	δ-MnO_2 amorphous	<50 nm	ED + cathodization	FTO	0.1 M KPi 7	~550 mV @ 1 $\frac{mA}{cm^2}$ [c]	0.1 $\frac{mA}{cm^2}$ @ 530 mV, 8 h [e]	[82]
26	δ-MnO_2 $K0.1MnO_x$ amorphous	150 $\frac{mg}{cm^2}$	Redox deposition	GS	0.066 M KPi 7	~660 mV @ 10 $\frac{mA}{cm^2}$ [a]	1.3 $\frac{mA}{cm^2}$ @ 540 mV, 16 h [d]	[109]
27	δ-MnO_2 $K_{0.1}MnO_x$ amorphous	165 $\frac{mg}{cm^2}$	Redox deposition	CFP	0.066 M KPi 7	~640 mV @ 10 $\frac{mA}{cm^2}$ [a]	1.7 $\frac{mA}{cm^2}$ @ 540 mV, 16 h [d]	[109]
28	δ-MnO_2 c-disordered	4 μm	ED + 300 °C	FTO	0.1 M KPi 7	~430 mV @ 1 $\frac{mA}{cm^2}$ [a]	8.2 $\frac{mA}{cm^2}$@ 580 mV, 20 h [d]	[74]
29	δ-MnO_2 c-disordered		ED + 300 °C	CNT + Ni-foam	1 M KOH 14	~430 mV @ 100 $\frac{mA}{cm^2}$ [a]	20 $\frac{mA}{cm^2}$@ 300 mV, 1 h [d]	[114]
30	δ-MnO_2 $K_{0.1}MnO_x$ amorphous	180 $\frac{mg}{cm^2}$	Redox deposition	CFP	1 M KPi 2.5	~580 mV @ 10 $\frac{mA}{cm^2}$ [c]	2 $\frac{mA}{cm^2}$ @ 510 mV, 24 h [e]	[131]

Tab. 2 (continued)

#	MnO_x cat. phase	Cat. mass/thickness	Dep. method	Substrate	Electrolyte pH	Performance	Stability	Ref.
31	δ-MnO_2 $K_{0.1}MnO_x$ amorphous	180 $\frac{mg}{cm^2}$	Redox deposition	CFP	1 M KPi 7	~560 mV @ 10 $\frac{mA}{cm^2}$ [c]	2 $\frac{mA}{cm^2}$ @ 500 mV, 24 h[e]	[131]
32	δ-MnO_2 $K_{0.1}MnO_x$ amorphous	180 $\frac{mg}{cm^2}$	Redox deposition	CFP	1 M KOH 14	~330 mV @ 10 $\frac{mA}{cm^2}$ [c]	2 $\frac{mA}{cm^2}$ @ 360 mV, 24 h[e]	[131]
33	δ-MnO_2 amorphous	4.4 $\frac{mg}{cm^2}$	ED	FTO	0.1 M KPi 7	~590 mV @ 1 $\frac{mA}{cm^2}$ [c]	instable @ 530 mV after minutes[d]	[49]

[a]Activity from cyclic voltammograms.
[b]Activity from cyclic voltammograms recorded with a rotating disk electrode (RDE).
[c]Activity from Tafel-analysis.
[d]Activity from chronoamperometry measurements.
[e]Activity from chronopotentiometry measurements.
ALD, atomic layer deposition; ED, electrodeposition; GC, glassy carbon; HAS, high surface area; FTO, fluorine doped oxide; GS, graphite sheet; CFP, graphitized carbon fiber paper; CNT, carbon nanotubes; KPi, potassium phosphate.

especially rewarding and phosphate buffers have proven to be a very good choice. Towards both alkaline and acidic media, MnO_x show remarkable stabilities and reasonable activities over the whole pH range, making these WOC catalysts true "all-rounders" suitable for many different applications and devices.

3.4 Structure/activity relationships for electrochemical WOC

The oxygen evolution reaction is a very complex four-electron/four-proton redox process involving multiple bond cleavages and the formation of the O–O double bond. A detailed understanding of WOC mechanisms exists only for two systems: molecular ruthenium catalysts like the "blue dimer" and the OEC, biology's $CaMn_4O_x$-cluster catalyzing water-oxidation in photosynthesis [143–147]. For heterogeneous catalysts like manganese oxides, on the other hand, our mechanistic knowledge is still in its infancy, so that even the nature of the WOC active sites in MnO_x catalysts is largely unknown. As a first indication, researchers try to correlate data about the bulk structures of metal oxides with their electrochemical WOC activities [148–152]. For the case that this leads to convincing results, it is then hoped to start a knowledge-guided search for more efficient catalysts. Generally, one has to admit that such a "rational catalyst design" is so far not possible for WOC by metal oxides. In the case of manganese oxides, however, there is a certain advantage: as biology "chose" a manganese-oxido cluster as WOC active site, an enormous wealth of information about this particular catalytic mechanism taking place at a MnO_x active site has been accumulated over decades of research [15, 20, 153–155] and can now be used for a better understanding of synthetic MnO_x catalysts as well.

Already some early studies dealing with the electrochemical performance of manganese oxides as water oxidation catalysts revealed a possible relationship between the MnO_x-phase and its WOC activity [37, 60]. As mentioned before, Tamura and co-workers prepared mixed MnO_2/Mn_2O_3-electrodes and investigated their catalytic performances in comparison with pure MnO_2 or Mn_2O_3. Interestingly, they found that the oxide mixture was more active than both pure phases on their own and concluded that both Mn^{3+} and Mn^{4+} centers might be involved in WOC. However, no evidence for this claim (e.g. from UV/Vis or X-Ray absorption spectroscopy) was available at this time.

Over the last decades, many research groups investigated possible correlations between manganese oxide phases and their catalytic activities and generally found large influences of the catalysts' bulk structures on WOC rates

[79, 92, 120, 122, 128]. For example, one of our teams systematically tested the electrocatalytic activities of electrochemically deposited amorphous manganese oxide (MnO_x/FTO, annealed at 573 K to increase its activity), Mn_2O_3/FTO and Mn_3O_4/FTO [79]. The latter two were obtained by further calcination steps from the amorphous MnO_x and showed high crystallinities, low surface areas (determined by capacitance measurements), but still significant film porosities. Even as all three manganese oxides acted as water-oxidation catalysts above $E = +1.8$ V in phosphate buffer at pH 7, clearly lower onset potentials and higher current densities were detected for MnO_x/FTO and Mn_2O_3/FTO (~570 mV at 10 mA cm^{-2}, see Figure 7). This was explained by structurally more flexible Mn-sites well suited for WOC (in the case of the amorphous MnO_x) and the especially low specific resistance of Mn_2O_3 (Table 1). These results are in line with numerous other studies which generally indicate that MnO [121, 122, 132], Mn_3O_4 [82, 97, 126, 128] or MnO_2-polymorphs [73, 92, 99, 120, 156], are generally less active in electrochemical WOC than Mn_2O_3 [61, 71, 79, 83, 119, 122, 128, 132] or amorphous (mostly layered) MnO_x [49, 72, 74, 75, 77, 81–83, 109, 120, 141, 157].

However, it is hardly possible to derive the nature of the catalytically active sites in such materials from analytical methods like XRD or SEM/TEM which characterize the bulk material's crystallographic phase or morphology. More advanced techniques like X-ray absorption spectroscopy (XAS) or X-ray photoelectron spectroscopy (XPS) were therefore used in a number of studies, especially for nanocrystalline or highly disordered systems, where diffraction methods yield little information.

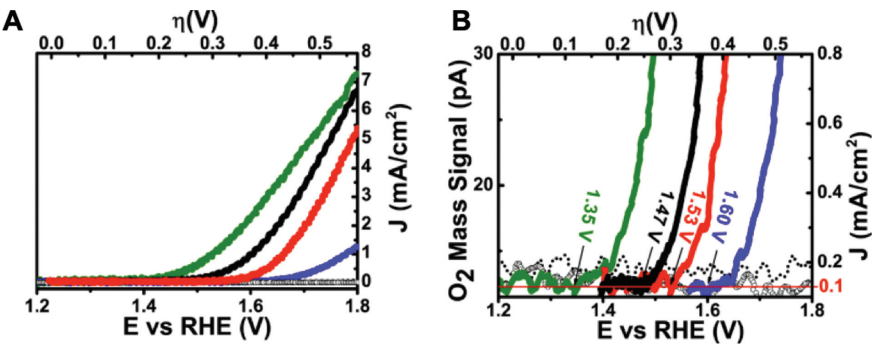

Fig. 7: (a) Current densities *J* and (b) oxygen mass signals (at low *J*) as a function of the applied potentials *E* for sputtered RuO_2 (green), amorphous MnO_x (dotted), amorphous MnO_x annealed at 573 K (red), Mn_2O_3 (black) and Mn_3O_4 (blue) films deposited on FTO (black open circles) in 1 M phosphate buffer (pH 7.0). Reprinted from Ref. [79] with permission by the American Chemical Society.

From the analysis of surface-sensitive analytical data (like XPS), several groups concluded that an amorphous MnO_x layer is often formed on top of crystalline oxide materials like Mn_2O_3 at WOC conditions [48, 79]. For example, in our study mentioned above (Figure 7) we detected an increase of the average Mn oxidation state from +3 to +4 at the surface of the Mn_2O_3 catalyst by XPS. Similarly, Gorlin et al. and also Lange and co-workers reported the formation of a less-ordered birnessite-like structure on the surface of MnO_x particles after an application of oxidizing potentials [116, 128]. These results were recently confirmed by Tesch et al. who showed by *in situ* Mn L-edge XAS studies that a birnessite was the catalytically dominant phase during water oxidation catalysis by a mixture of Mn_3O_4/Mn_2O_3/birnessite at potentials $E > 1.45$ V. Furthermore, resonant inelastic X-ray scattering (RIXS) indicated that Mn oxidation never seems to exceed the +4 state, but rather that a partial $O \longrightarrow Mn^{IV}$ charge transfer seems to occur at high oxidation potentials [85].

A detailed study concerning the WOC active sites of MnO_x materials for the subsequent development of rationally designed catalysts was carried out by one of our groups in 2012 [49]. The structural parameters of a WOC-inactive and an active MnO_x film, obtained from UV/Vis and Mn K-edge XAS measurements, were compared. Both materials were characterized as amorphous MnO_x exhibiting slightly different morphologies but roughly identical surface areas. The average oxidation states of the two samples differed and were estimated to be +3.8 for the active and +4.0 for the inactive material. Furthermore, the shape of the X-ray absorption near-edge structure (XANES) spectrum revealed that the inactive film was composed of a regularly assembled, layered birnessite-type MnO_x, whereas the active oxide exhibited a higher disorder and a more heterogeneous ligand environment. These conclusions were supported by the information gained from extended X-ray absorption fine structure (EXAFS) spectra, in which both materials are found to be built up from $Mn^{III/IV}O_6$-octahedra. However, while these building blocks are mainly connected via di-μ-oxido bridges to form a well-ordered layer in the inactive oxide, the active catalyst contains many mono-μ-oxido bridged Mn ions, resulting in a lack of long-range order (Figure 8). From this observation it was concluded that layered $Mn^{III/IV}O_x$ of low order with many terminal coordination sites for reactive water species show high water oxidation activities, while in well-ordered MnO_x such readily (de)protonatable μ_2-O(H) groups are not available as WOC active sites. The special importance of bridging oxido ligands for WOC has also been noted for other metal oxides like CoO_x or NiO_x and is also a central feature of WOC by the OEC [146, 148, 149, 151, 152, 158–161]. Finally, DFT calculations in combination with XAS data also confirmed that more active MnO_x films are formed by the interconnection of small, planar Mn-oxido sheets cross-linked by out-of-plane Mn atoms introduced by disorder, which can be arranged in closed cubane-like units very similar to the one found in the OEC [162].

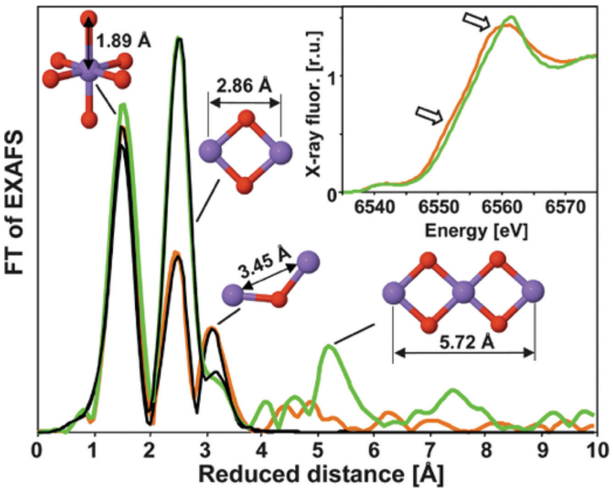

Fig. 8: X-ray absorption spectra of an WOC active (orange) and inactive (green) MnO_x. The inset shows the edge region of the spectrum (XANES), from which the average oxidation state of the Mn ions was estimated by a comparison with Mn reference compounds. Each peak in the Fourier transformed EXAFS spectra relates to a specific structural motif that is schematically depicted (O in red, Mn in purple). The spectra obtained by EXAFS simulations are shown as black lines. Reprinted from Ref. [49] with permission by the Royal Society of Chemistry.

In a further set of experiments, one of our teams compared the oxidation state and structural dynamics of an active, an inactive and a Ca^{2+}-doped MnO_x film with the biological catalyst by means of electrochemical quasi *in situ*, freeze-quench XAS complemented by time-resolved detections of XAS, UV/Vis and impedance spectra (Figure 9). The combined data revealed changes of the average Mn oxidation state upon the application of a WOC potential from around $+3.4$ to $+3.9$, which is comparable to the changes known for the OEC during operation [93]. Such changes of the average Mn oxidation state during and/or after operation have also been found in other studies [73, 77, 128]. Interestingly, the inactive MnO_x film reached an all-Mn^{4+}-state while for the active film some residual Mn^{3+}-ions were found even after extended operation at $+1.45$ V. We propose that these trapped Mn^{3+}-states are essential for the formation of structurally highly flexible local clusters that could resemble the active sites of water oxidation catalysis. Additionally, we would like to stress that this study again indicates that the stabilization of a fraction of Mn^{3+}-centers at water oxidation potentials seems to be decisive for catalytic activity.

In summary, amorphous or nanocrystalline, highly disordered and often layered manganese(III, IV) oxides seem to be especially well suited for electrochemical water oxidation. These materials show an ability to accumulate oxidizing equivalents by bulk oxidation state changes and might contain functional units

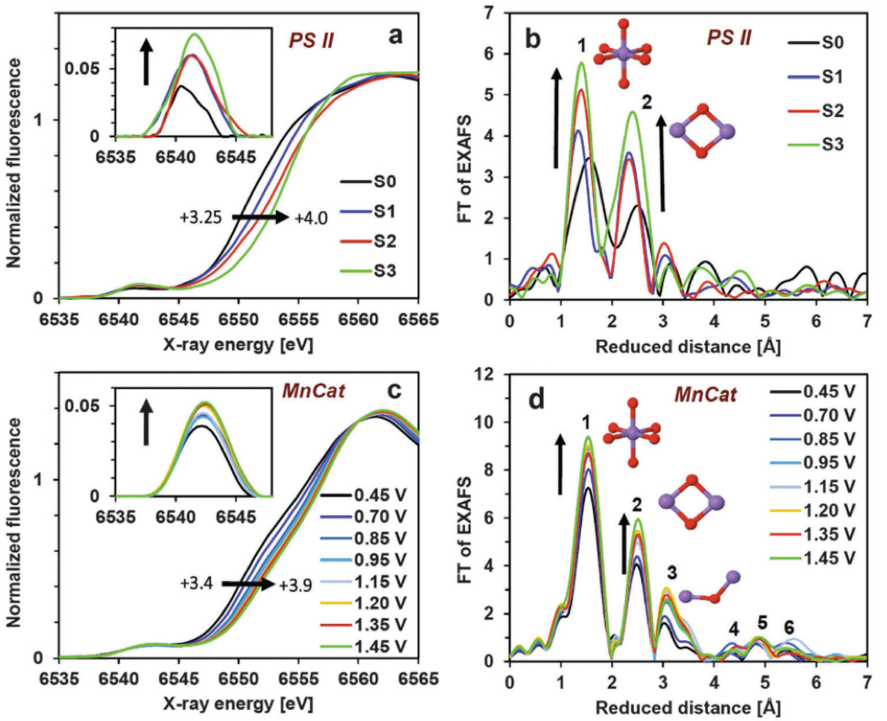

Fig. 9: XANES and EXAFS spectra of the OEC within the enzyme complex Photosystem II and of an electrodeposited active MnO_x. (a) XANES and (b) EXAFS of the Mn_4Ca complex for the four semi-stable intermediates of the S-state cycle. (c) XANES and (d) EXAFS of electrodeposited MnO_x where oxidation state changes were induced by the indicated potentials (given vs. NHE). For each FT peak the corresponding structural motif is schematically shown (Mn: magenta, O: red). Reprinted from Ref. [93] with permission by the Royal Society of Chemistry.

of molecular dimensions (like metal oxido-cubanes) as also found in the OEC. Additionally, they also often feature beneficial materials properties like high surface areas and/or porous structures.

4 Electrode performance vs. operation parameters

Thus far, we have presented overviews about parameters like conductive supports, deposition methods, electrolyte variations and MnO_x phases, all of which influence electrochemical WOC by manganese oxides. The following

section will now address the overall performance of MnO_x anodes at different operation conditions. For this, we compare the influence of the individual parameters mentioned above on two performance indicators, namely (1) the overpotentials necessary to reach a certain current density (mainly obtained from CV measurements) and (2) the change of this value over time observed in long-term electrolysis experiments (Table 2). At this point it has to be mentioned that such a comparison is complicated by the fact that different groups use different electrochemical testing protocols (often – but not always – for a good reason) and that a standardization of such performance measurements (though sometimes tried) is so far lacking in this field [163–165]. Furthermore, the measured electrochemical currents are mostly normalized to the geometric surface areas (instead of using mass activity data and/or layer thickness dependencies) and especially in the cases of high surface area backbones and/or porous catalyst layers (like many MnO_x) the macroscopic geometrical areas are for sure much smaller than the electrochemically active surface areas. Finally, in most studies it is assumed that the entire current observed at high potentials is the result of water-oxidation to molecular oxygen. For long-term electrolyses, this assumption has been proven to be mostly correct by determining the Faradaic O_2 yield [77, 81, 109]. However, for CV experiments on freshly prepared electrodes it is known that other processes like Mn-centered oxidations, reactions of the support material or capacity effects greatly contribute to the detected currents so that one has to be especially careful when comparing anodes for which only CV data is available [67, 87]. Despite all these uncertainties, we think that by now enough data on the WOC performance of MnO_x electrodes exists to derive some general trends.

As already discussed above, many different MnO_x phases exist and most have also been tested in detail as potential anode materials for the electrocatalytic OER. From the results listed in Table 2, MnO, α-Mn_2O_3, Mn_3O_4, γ-MnO_2 (ramsdellite) and δ-MnO_2 (birnessite) emerge as the most popular choices, and all these oxides have shown significant WOC activity. On the other hand, a closer look at Table 2 also reveals that activity and stability cannot easily be derived from the MnO_x phase alone. Firstly, other parameters like deposition method or support material also play important roles (see below). Another already mentioned important point are the often observed transformations and amorphization of the as-prepared MnO_x material to "catalytically active phases" when WOC potentials are applied. For example, different groups have reported nearly identical overpotentials ($400 < \eta < 500$ mV) needed to reach 10 mA cm^{-2} under strongly alkaline conditions (pH >12), even though the oxides initially deposited on the electrode were characterized to have largely different bulk Mn oxidation states and/or structures (MnO, Mn_3O_4, α-Mn_2O_3, δ-MnO_2, γ-MnO_2 or β-MnO_2, please note: only catalysts on flat substrates were considered) [61, 73, 120, 122, 132]. An in our view likely

explanation for this fact could be the transformation of all these starting materials (at least at the surface) into the same catalytically active phase. Judging from a number of studies, we suspect that this active phase is most likely best described as an amorphous MnO_x with a layered structure (birnessite-type) and this has also been confirmed experimentally in some studies [82, 85, 132]. To support this conclusion, we would also like to point to the fact that birnessites (closely followed by α-Mn_2O_3) are the "most popular" MnO_x starting materials in our list of promising MnO_x anodes, indicating that these oxides are commonly seen as the most active MnO_x (pre)catalysts currently available for WOC.

As already stated above, the different MnO_x catalysts have also been tested over the entire pH range from strongly acidic to highly alkaline conditions. First and foremost, it is worth to mention that MnO_x are indeed able to act as electrocatalysts for water-oxidation from pH ~1 to pH ~14, where as all other metal oxides used in WOC are usually limited to much smaller pH windows (see below). As a general trend, higher activities have generally been observed for highly alkaline conditions (typically 0.1–1 M (K,Na)OH), where the best MnO_x anodes reach a current density of 10 mA cm^{-2} at overpotentials η = ~350 mV (Table 2, see entries 8 and 32). This trend of a greatly facilitated OER under alkaline conditions is in line with the findings for other transition metal oxides and most likely has its origin in the efficient removal of protons from WOC active sites by the very efficient base OH^- and/or (so far not understood) changes of the catalytic mechanism [163, 166, 167]. Under neutral conditions, the best electrodes generally require higher overpotentials of η = ~450–550 mV to reach benchmark activities of 1–10 mA cm^{-2} (Table 2, see entries 3, 7, 21 or 31), respectively. Nevertheless, it should be stressed that these catalytic performances of MnO_x anodes are among the best that have been reported for non-precious metal oxides at pH ~7 [11, 136, 168]. Finally, the ability to catalyze the OER with remarkable stabilities even under acidic conditions (η = ~500 mV, see entries 17, 24 or 30) is a property that makes MnO_x unique in comparison with other abundant OER catalysts like CoO_x or NiO_x. Especially recent work by Nakamura and co-workers, in which γ-MnO_2 was found to be able to sustain a WOC current density of $j = 10$ mA cm^{-2} at pH 2 for more than 8000 h, impressively demonstrates that MnO_x catalysts might be a promising, earth-abundant alternative to IrO_x or RuO_x, the currently most commonly used water-oxidation catalysts under acidic conditions (e.g. in PEM electrolysers) [103, 141].

The great impact of the substrate's surface morphology can be seen in a study by Pickrahn et al., where a MnO (pre)catalyst was deposited via ALD on two types of glassy carbon substrates, one with a smooth and another with a much larger, rough surface (high surface area glassy carbon, HSA-GC) [122, 132]. Capacitance measurements were taken as a measure for the size of the electrolyte/electrode

contact area and showed that the accessible surface of MnO/HAS-GC was about five times larger than that of MnO/GC. The WOC activities at pH ~13 fitted this difference in surface areas very well as a nearly five-fold increase of the current density was observed for the anode with the rougher surface (23 vs. 5 mA cm^{-2} for $\eta = \sim 500$ mV). A similar trend was observed by one of our groups when we compared the WOC performance of a birnessite deposited on a high surface area graphitized carbon fiber paper to that of the same catalyst on a planar, smooth graphite sheet (Table 2, see entries 26 and 27): in long-term experiments at $\eta = 540$ mV and pH 7, the current density for CFP as a substrate was ~30% higher than that for GS (1.7 vs. 1.3 mA cm^{-2}, respectively) [109]. Sun and co-workers went even one step further and decorated the already large surfaces of Ni-foam (NF) substrates with CNTs by electrophoresis [114]. The resulting conductive substrate with an extremely high ECSA of 1000 cm^2 per cm^2 of geometric area was afterwards decorated with c-disordered birnessite by electrodeposition. In 1 M KOH, the resulting MnO_x/CNT/NF-construct with an estimated ECSA of 30.000 cm^2 showed a record-setting geometric current density of $j = 100$ mA cm^{-2} at a low overpotential of only $\eta = 330$ mV, thus demonstrating the great potential of such a high surface area electrode architecture (*note*: although it was ruled out in this study, Ni itself can be converted into an excellent OER electrocatalyst under strongly alkaline conditions and could therefore contribute to the high activity).

For amorphous, porous MnO_x materials it is possible to increase the ECSA simply by depositing thicker catalyst layers and hence higher catalyst loadings and this also results in more active electrodes, as shown by different groups [61, 73, 77, 83, 121]. In a study by some of us, electrodes with different thicknesses (0.5, 1.2, 3.6, 9.6 and 15 μm) were prepared by screen-printing of an ink containing a porous Ca-birnessite of high specific surface area onto FTO [77]. The highest WOC current densities at pH 7 were found for catalyst layers with a thickness of 10 μm, which in the field of catalytically active films is a very high value. Both thinner and thicker layers showed 2–4 times lower activities. This might be explained by an optimized ratio between the number of active sites (more in thicker films) and the distance electrons have to be moved through the catalyst to reach the conductive support (longer for thicker films), respectively. Similar results were found by Spiccia and co-workers [73] and Kölbach et al. [61] who also tested the influence of the film thickness on the activity. Recently, our groups optimized the mass loading of a chemically deposited birnessite on CFP supports and found six-fold higher current densities (3 vs. ~0.5 mA cm^{-2} for $\eta = 450$ mV and pH 7) when the Mn loadings where increased from 1 to 16 μmol cm^{-2} (Figure 10). On the other hand, the fact that 16 times more catalyst was needed to enhance the catalytic current by a factor of only 6, indicates that the normalized activity per Mn ion is decreased

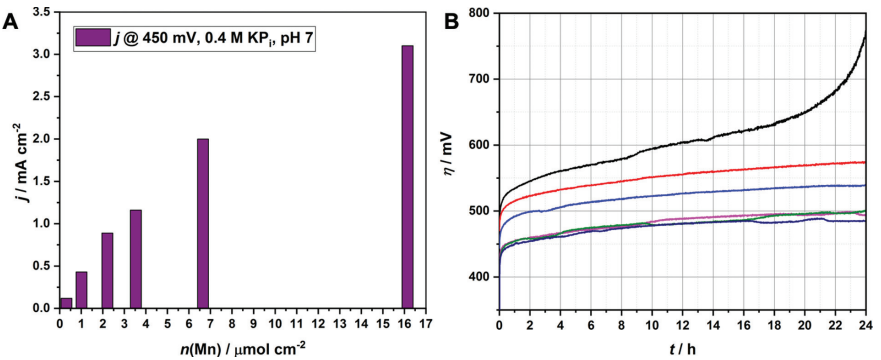

Fig. 10: Current density j (a) for an overpotential $\eta = 450$ mV and (b) long-term stability measurements at a constant current density $j = 2$ mA cm^{-2} over 24 h for K-birnessite/CFP-electrodes functionalized with different amounts of Mn-ions (0.3 μmol cm^{-2} = black, 1.0 μmol cm^{-2} = red, 2.2 μmol cm^{-2} = blue, 3.7 μmol cm^{-2} = pink, 6.6 μmol cm^{-2} = green, 16.6 μmol cm^{-2} = dark blue). All measurements were conducted in 0.4 M KP$_i$ at pH 7 [131].

at higher catalyst loadings [131]. Hence, long-term experiments revealed that for higher and higher amounts of MnO_x, the activity is found to saturate at a maximum value (Figure 10). Finally, it should also be mentioned that thicker catalyst layers also suffer less from corrosion, especially under neutral to acidic conditions where the stability of the catalysts is generally a bigger issue [49, 122]. This is most likely due to the fact that due to the higher geometric activity, lower potentials can be applied to reach a distinct current density. Resulting in milder operating conditions. Thus, the development of thicker, porous catalyst layers has led to MnO_x anodes which can be operated at $j > 1$ mA cm^{-2} without loss of activity for hours or even up to months [141].

In summary, the "ingredients" for a well-performing, MnO_x-based water-oxidation half-cell of an electrolyzer might be defined as such: (1) a suitable catalyst material, where especially α-Mn_2O_3 and birnessite-type MnO_x have proven to be promising candidates; (2) a conductive support material with a high intrinsic surface area like carbon fiber paper, CNTs or Ni-foam; (3) a rather thick, porous catalyst layer (high MnO_x mass-loading) resulting in a large number of accessible active sites and (4) an optimized electrolyte composition. On the last point, MnO_x can reach high activities and stabilities over the entire pH range from strongly alkaline via neutral even to acidic conditions. The improvements in performance achieved for MnO_x-based WOC mainly by working on these four parameters are in our view impressive so that we are convinced that MnO_x-anodes are hot candidates for future applications in electrochemical energy conversion devices.

5 Outlook: possible applications of MnO_x electrodes in technical devices

The previous sections provided an overview about MnO_x based water-oxidation catalysts, the preparation and use of MnO_x-electrodes for electrochemical WOC and important factors influencing the activity and stability during operation. Although many open questions remain, we will now nevertheless try to give an outlook concerning a central question for this research field: *"Are manganese oxides suitable materials for a technical application as water oxidation catalysts?"*

Figure 11 shows three common designs of devices for "artificial photosynthesis" or "renewable fuels". All resemble electrochemical cells where MnO_x-electrodes could possibly be used as OER catalysts, but otherwise each device-type requires different operation conditions which in each case influence the choice of catalyst-materials.

Alkaline electrolysis cells (AECs) have been industrially used since the 1920s and represent the most mature electrolyser technology available for the production of H_2 today. If used on an industrial scale, AECs are composed of two electrodes immersed in a strongly alkaline electrolyte (usually ~20–30% KOH) and separated by a diaphragm. The AEC is normally operated using cell voltages of ~1.8–2.0 V and iron-doped nickel oxides ($NiFeO_x$) are commonly used as anode materials, as these show high activities for low overpotentials and remarkable long-term stabilities at such "AEC conditions" (see also Figure 12)

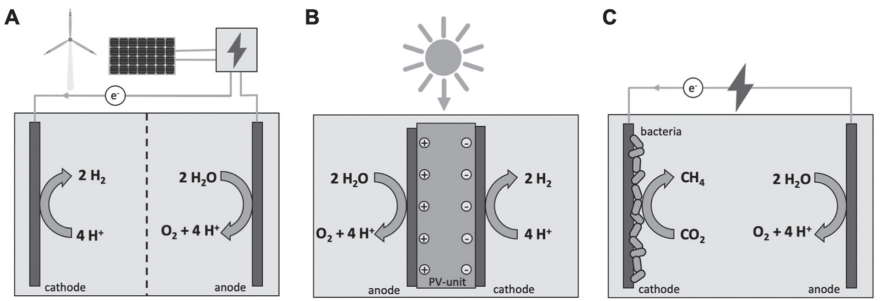

Fig. 11: Schematic representation of three common designs for the renewable-energy-driven production of fuels like H_2 or CH_4. (a) Alkaline (AEC) or polymer electrolyte membrane (PEMEC) electrolysis cells coupled to the electricity grid which will in the future mainly be fed by renewable energy sources; (b) fully integrated, wireless photoelectrochemical devices ("artificial leaves"), where the catalysts are in close contact with light-absorber materials; (c) microbial electrosynthesis cells (MESCs), in which the reducing equivalents obtained from the OER are used by bacteria immobilized on the cathode to produce carbon-based fuels or raw materials from CO_2.

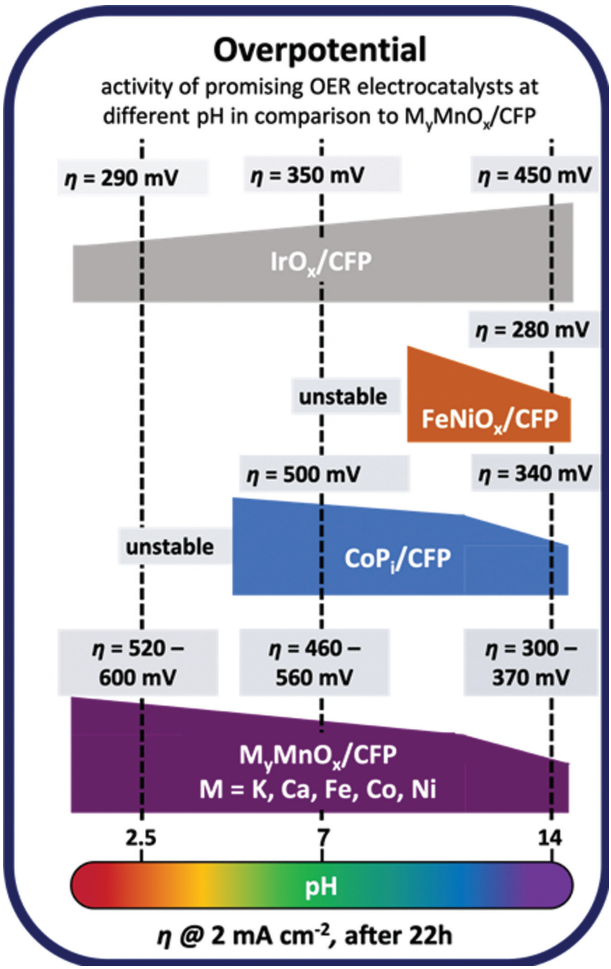

Fig. 12: Activities and stabilities of promising materials for OER electrocatalysis at different pH conditions [169]. Please note: for better comparison all catalyst materials have been deposited on a carbon fiber paper substrate by electrodeposition after literature known procedures (IrO_x [170], $FeNiO_x$ [171], CoP_i [172], MnO_x [109]).

[103, 169, 173–175]. Even though manganese oxides are also most active and stable in strongly alkaline electrolytes, their performances are far inferior to the outstanding results observed for $NiFeO_x$ at pH >12. As both Ni and Fe are also abundant elements, it thus seems very unlikely that MnO_x will be able to replace $NiFeO_x$ as anode material of choice in AECs.

Despite decades of industrial optimization, AECs still have some major disadvantages such as low maximum current densities of 0.2–0.4 A cm^{-2} due to

ohmic losses (mainly by the diaphragm), bulky stack configurations and a limited ability to respond to voltage fluctuations, the latter being especially problematic if electricity from renewable sources like wind or solar is driving the AEC [103]. Electrolysers based on a solid polymer electrolyte concept like proton exchange membrane or polymer electrolyte membrane electrolysis cells (PEMECs) avoid most of these issues. PEMECs can be operated at much higher current densities of up to 2 A cm^{-2} due to the high proton conductivities of the membranes at acidic pH values (pH ~2). Furthermore, PEMECs show fast proton transport across the membrane which allows them to work under a wide range of power inputs and to react rapidly to electricity fluctuations [176, 177]. However, few catalyst materials are stable at the applied voltages (1.8–2.2 V) and the corrosive acidic regime where PEMECs show their best performances. The only convincing WOC materials for these operating conditions available today are based on the scarce and expensive elements Ru and Ir, as both RuO_x and IrO_x show very high activities and good stabilities under strongly acidic conditions (see also Figure 12) [178–180]. Interestingly, manganese oxides are the only currently investigated abundant transition metal oxides which show decent stabilities at pH <7 (unlike $FeNiO_x$ or CoP_i, see Figure 12). However, it has to be admitted that even for low WOC current densities, MnO_x require high overpotentials at pH ~2. Nevertheless, we see a clear potential here and recommend to investigate MnO_x or also multinary Mn-based compounds like $NiMnSbO_x$ more closely as possible substitutes for RuO_x and IrO_x anodes in PEMECs [138].

"Artificial leaves" or photoelectrochemical cells (PECs) are water splitting devices in which the catalyst materials for water oxidation and product formation are in direct contact with the surfaces of a semiconductor material used for light-driven charge separation (see Figure 11b) [2, 181, 182]. Due to this architecture, the current densities reached by artificial leaves are generally 20–100 times lower when compared to classical electrolyzer technologies. This can be explained by the fact that usually two to three absorber materials have to be connected in series to reach potential differences sufficient to drive water-splitting. Such "tandem" or "triple-junction" semiconductor arrangements generate photovoltages of >1.8 V, but maximum current densities of only ~10 mA cm^{-2} [183, 184]. Taking this into consideration, MnO_x might well offer the performance required for OER catalysts in artificial leave devices. For this, the good performances of MnO_x at intermediate pH values are again a major advantage, as it has so far proven to be very difficult to fully avoid corrosion problems when artificial leaves were operated at the very acidic or very alkaline conditions typical for commercial water-electrolysis cells.

Similarly, microbial electrosynthesis cells (MESC, Figure 11c) might be another interesting type of devices where MnO_x could be used as OER catalysts. In a MESC, the reducing equivalents that are gained from the oxidation of water

are used by bacteria which are immobilized on the cathode to produce valuable, carbon-based substances from CO_2. Several studies have demonstrated that it is possible to obtain compounds like acetate, 2-oxobutyrate, methane or ethanol via microbially catalyzed synthesis in such cells [185–190]. However, this setup results in some special requirements for the OER half-cell: (1) the reaction medium regularly contains chloride as this anion is essential for microorganisms. Therefore, the anode must show a high selectivity for the oxidation of water over the oxidation of chloride ($E_{(Cl^-/Cl_2)} = 1.36$ V) because Cl_2 or oxochlorides like OCl^- are highly toxic for most microorganisms [191]; (2) not all metals can be used as their leaching into the reaction medium can lead to the inhibition of microbial growth, as recently shown for Ni [192, 193]; (3) again, the electrocatalyst needs to be stable and active in the intermediate pH regime as a neutral environment is commonly required for biological growth. Manganese oxides could well meet all three requirements as they (1) generally show high overpotentials for the chlorine evolution reaction and for that reason have even been used in seawater electrolysis [194–196], (2) are non-toxic for most organisms and 3) show good OER performances around pH 7. Consequently, we conclude that MnO_x anodes should be very suitable for a use as anodes in a microbial fuel cell.

Overall, in our opinion MnO_x anodes for WOC are very promising candidates for applications in devices which are operated at low current densities ($j \leq 10$ mA cm^{-2}) and near neutral pHs such as artificial leaf devices or MESCs. Furthermore, we could see potential applications in PEMECs as a substitute for the expensive (Ru, Ir)O_x catalysts, but only if the activities can be significantly increased while maintaining the remarkable stability at low pHs. On the other hand, an application of MnO_x in AECs as a possible replacement for the commonly used $FeNiO_x$ catalyst materials seems improbable.

6 Epilogue: why did nature “choose” manganese for water-oxidation catalysis?

One of the main conclusions of this review has been that manganese oxides are good, but in most cases clearly not the best materials for water-oxidation catalysis. Thus we finally turn to a second fundamental question, which has already been formulated by Fraser Armstrong in a paper published about 10 years ago: *“Why did Nature choose manganese to make oxygen?”* [197]. To address this question, we will use an unconventional and, admittedly, speculative line of argument. Rather than focusing immediately on specific chemical properties of manganese, we start by summarizing crucial properties of the manganese complex of photosynthetic

water oxidation. Then we will argue that not only amorphous manganese oxides but also water-oxidizing materials based on some other transition metals resemble the biological catalyst in its crucial properties. Consequently, we hypothesize that also further transition metals might have been employed for biological water oxidation, but were outcompeted by manganese merely because of the higher abundance of dissolved Mn^{2+} ions in the earth's surface waters.

6.1 What does the biological OER catalyst – the OEC – look like?

In biology, light-driven water oxidation is catalyzed by means of high-valent manganese ions bound to the proteins of photosystem II (PSII) [14, 19, 161, 198–200]. Most likely, all photosynthetic organisms capable of water oxidation, that is, all plants, algae and cyanobacteria, are using a highly similar machinery and specifically the same metal cluster for WOC. The core of the biological catalyst is a compact $Mn_4^{III/IV}Ca(\mu_3\text{-}O)_4(\mu_2\text{-}O)$ moiety (where μ_2-O and μ_3-O indicate an oxygen atom in bridging position between 2 and 3 metal ions). Its structure may be conceived as a small fragment carved out of an extended manganese calcium oxide, e.g. from the mineral marokite ($CaMn_2O_4$) [57]. In line with this "oxide character"

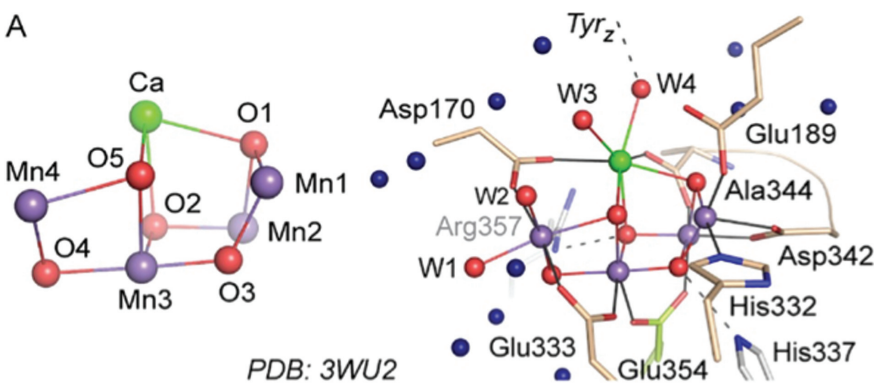

Fig. 13: The core of the manganese-calcium-oxido cluster (left) and the surrounding protein groups (right) of photosystem II (PSII) in its dark-stable state [201]. We note that Glu189 also may be conceived as being a calcium ligand. However, because the distance between the calcium ion and O-Glu189 is comparatively long, no bond is indicated here. One of the terminal water ligands (W4) is in hydrogen-bonding distance to a specific tyrosine residue denoted as Tyr_Z. Illumination of PSII causes oxidation of Tyr_Z, which then drives a $Mn^{III} \rightarrow Mn^{IV}$ oxidation step in at least three of the five redox transitions of the classical PSII reaction cycle (S-state cycle). The dark-blue spheres indicate protein-internal water molecules, which are part of an extended H-bonded protein-water network. (Graphic from Ref. [202] copyright comment: licensed under CC BY 4.0; URL: https://elifesciences.org/articles/26933.)

of the biological catalyst, all further donor atoms to Mn and Ca are also oxygens (with the exception of the nitrogen atom N-His332, see Figure 13) [201, 203], as a further four water or hydroxide molecules are terminally coordinated to Mn1 (W1, W2) and the calcium ion (W3, W4) [201, 204]. Looking beyond these first-shell ligands, we find that the Mn_4Ca-oxido cluster is partially surrounded by protein ligands and partially by a protein-internal water cluster comprising, inter alia, the terminal water ligands of the Mn1 and the Ca ion. Grossly simplified, the catalytic site of biological water oxidation consists of a tiny manganese-calcium oxide of well-defined structure anchored by protein ligands and partially exposed to water (which is both solvent and substrate of the water oxidation reaction).

6.2 What determines the specific structure of the OEC's oxide core and how is it formed?

The metal-oxido core is formed in a process that may be denoted as oxidative self-assembly, but traditionally is called "photoactivation" in photosynthesis research [205]. Driven by light, a redox-active tyrosine residue of PSII called Tyr_Z is oxidized and in turn oxidizes Mn^{2+} ions that need to be present, at low concentrations, in the solvent environment of PSII. The oxidation of four Mn^{2+} ions eventually yields four $Mn^{III/IV}$ ions, which are bound to the protein and interconnected by di-μ-oxido bridges. However, unlike in synthetic oxides, nuclearity and structure of this metal-oxido core are determined by ligands from the protein's side-chains. Six carboxylates serve as bidentate ligands bridging between two metal ions each, complemented by one monodentate imidazole ligand (His332, Figure 13). In the absence of the Mn_4Ca-cluster, these ligating, evolutionary conserved residues are arranged in almost the same way as in its presence, suggesting that the structure of the apoprotein shapes the metal-oxido core [202]. On the other hand, it was recently reported that a synthetic complex closely resembling the OEC in structure, oxidation and spin states can also be prepared without the use of a complex ligand system [25]. A notable difference between this synthetic complex and the OEC is the absence of an open coordination site at Mn1, which is mostly believed to play a crucial role in biological water oxidation. Indeed, the synthetic compound is not active in WOC. Changes of UV/Vis absorption spectra suggest that spurious amounts of water cause a structural modification possibly associated with WOC activity, but clear evidence on the character of the structural change and its relation WOC activity is lacking [25].

In conclusion, the OEC is formed from dissolved Mn^{2+} ions by means of an oxidative self-assembly process in which details of its structure are determined by the specific protein environment. Similar structures may also form in the absence

of a complex ligand system, either via conventional preparation routes for molecular coordination compounds or during the (electro)synthesis of amorphous manganese oxides, as already discussed above. We note that all electrodeposition protocols and many other synthesis protocols for obtaining manganese oxides may be viewed as oxidative self-assembly processes, so that there is no basic conceptual difference compared to the OEC's assembly during photoactivation.

6.3 Accumulation of oxidizing equivalents by Mn – a mechanistic principle in biological WOC

In many mechanistic models of electrochemical water oxidation, the direct stepwise oxidation of water molecules (i.e. $[O^{2-}] \rightarrow [O^{-}] \rightarrow [O]$) has been assumed [146]. This involves, inter alia, that two "$[O^{-}]$"couple to a peroxide species before two further oxidation steps transform the peroxide into a dioxygen molecule. Moreover, typically this is assumed to happen at the surface of well-ordered transition metal oxides, which are largely inert regarding changes in atomic structure, protonation states of bridging oxides and metal oxidation states. Whether this type of model correctly describes electrochemical water oxidation by electrocatalytic materials is debatable – but this is not the subject of the present review. In PSII, a clearly different mechanistic paradigm is now generally accepted: three oxidation equivalents are sequentially accumulated by oxidation of manganese ions; once a fourth oxidation equivalent is available at the nearby tyrosine, the final water-oxidation/O_2-formation step of the catalytic cycle starts [14, 161, 199, 200]. Also in PSII research, the formation of oxyl radicals or peroxide species at earlier steps of the catalytic cycle has been discussed for decades [206–209], but it is incompatible with the now largely undisputed spectroscopic results on the oxidation-state changes of manganese ions in PSII [210–216].

6.4 Two crucial properties of the OEC

In this review, it is not possible to cover all properties of the OEC relevant for its function. Instead, we will focus on (a) the energetics (redox potentials) and (b) the role of the electronic coupling between metal ions facilitated by di-μ-oxido bridges.

a) In PSII, the oxidized (radical) form of a redox-active tyrosine (Tyr_Z^{ox}) serves as the oxidant driving water-oxidation catalysis. Its midpoint potential ($E_0{}^{TyrZ}$) has been estimated to be +1.1–1.2 V at pH ~5.5, which consequently constitutes a strict upper limit for the metal-ion oxidation potential ($E_0{}^{M/M^+}$) in the process of accumulating oxidation equivalents [14, 217]. However, too low potentials for $E_0{}^{M/M^+}$ could also be detrimental, because a large potential difference

$E_0^{TyrZ} - E_0^{M/M^+}$ would correspond to large energetic losses for the respective oxidation steps. Therefore, typical values of E_0^{M/M^+} within a rather narrow window below 1.1 V (E_0^{TyrZ}) and above 0.9 V (thermodynamic water-oxidation potential at pH ~5.5) are required for light-driven WOC in PSII.

b) For an efficient O–O bond formation step, the accumulation of oxidizing equivalents by spatially separated and electronically decoupled metal ions would be problematic, because oxidizing equivalents accumulated by electronically insulated metal ions could hardly support the concerted four-electron chemistry of the water-oxidation/O_2-formation step. Although systematic experimental and theoretical studies on this point are largely lacking, we hypothesize that di-μ-oxido bridging facilitates the needed electronic coupling between the individual metal sites. However, there also is a downside to electronically strongly coupled metal sites: a one-electron oxidation step of the metal cluster would raise E_0^{M/M^+} for a second oxidation step to a prohibitively high level (by several 100 mV). This can be prevented by appropriate coupling to charge-compensating deprotonation or other modifications of ligand groups, as discussed in more detail elsewhere [199, 218]. Prime candidates for such potential-lowering steps are the deprotonation of terminal water ligands as well as the transformation of μ-OH to μ-O ligands, as likely occurring in the S_0—S_1 transition of the biological metal cluster.

6.5 Comparison of biological WOC with WOC by transition metal oxides

So far, we have outlined crucial structural and functional properties of the biological catalyst for water oxidation in PSII. On these grounds we would now like to highlight some striking similarities of the OEC to (some) synthetic manganese oxides that are active in WOC:

(i) highly disordered MnO_x of the birnessite or todorokite type are very active catalysts and also share crucial structural motifs with the OEC [49, 55, 59, 93, 94].

(ii) active MnO_x can be synthesized (inter alia) by electrodeposition, a process that may be described as oxidative self-assembly. Similar to the self-assembly of the OEC, it also involves the oxidation of dissolved Mn^{2+} to $Mn^{3+/4+}$ ions and often results in a material rich in internal water molecules and stabilized by extensive di-μ-oxido bridges between $Mn^{3+/4+}$ ions [49].

(iii) Manganese oxides which are active in WOC can accumulate oxidizing equivalents by oxidation of Mn^{3+} to Mn^{4+} ions, a process which is most likely coupled to charge-compensating deprotonation steps also involving a rearrangement of the μ-oxido bridges between $Mn^{3+/4+}$ [93].

(iv) in spite of a beneficial influence of Mn^{3+} ions on WOC reaction rates, it is likely that the O–O bond formation step is taking place between O-atoms bound to Mn^{4+} ions.

Despite this remarkable set of similarities, the overpotential requirements of synthetic MnO_x for reasonable water-oxidation rates (η ~400 mV) are still significantly higher than that of the biological catalyst (at least in the near-neutral pH regime), which points towards unnecessarily high redox potentials ${E_0}^{M/M^+}$ in the synthetic oxides. Moreover, the formation of the specific structural motifs that facilitate fast water oxidation may be a rare (statistical) event, so that the actual number of WOC active sites in MnO_x catalysts might be quite low [93]. Though details are so far unknown, it is likely that these active sites contain Mn^{3+} ions also at catalytic potentials [93]. A key property of the specific, evolutionary optimized environment of the OEC in the protein may also be the optimal tuning the Mn^{3+}/Mn^{4+} redox potential and this might be one aspect explaining the OEC's exceptional catalytic performance.

In the last decade, there have been numerous fruitful investigations of WOC by first-row transition metal oxides (or oxyhydroxides) using a combination of electrochemical methods and X-ray spectroscopy at the respective metal K-edges. Most of these studies focused on catalyst materials based on CoO_x, (Fe)NiO_x and MnO_x (plus binary oxides). Above, we have already summarized the structural and functional similarities between biological water-oxidation by the OEC and WOC by MnO_x. Surprisingly, all the listed similarities, (i)–(iv), have also been found for amorphous cobalt and (iron) nickel oxides, which in addition also exhibit local structures and oxidation state changes of the metal ions similar to WOC-active MnO_x [10, 146, 149, 158, 219–225]. In clear contrast, amorphous iron-only oxides (FeO_x) do not exhibit these similarities and are WOC-inactive.

The common features of amorphous oxides (or oxyhydroxides) of manganese, cobalt or nickel can be explained by scrutinizing the midpoint potentials of the relevant redox transitions. In these catalyst materials, the potentials of the $M^{2+} \rightarrow M^{3+}$ and $M^{3+} \rightarrow M^{4+}$ transitions are typically only slightly above the equilibrium potential of water oxidation. There is still a significant uncertainty in the precise values of these potentials, but all three MO_x catalysts seem to be able to accumulate oxidizing equivalents via the formation of a sizeable fraction of M^{4+} ions at potential within about 200–500 mV above the equilibrium water-oxidation potential. In clear contrast, the $Fe^{2+} \rightarrow Fe^{3+}$ transitions in (WOC-inactive) FeO_x materials proceed far below the water-oxidation equilibrium potential and the $Fe^{3+} \rightarrow Fe^{4+}$ seemingly is not reached within a potential range that is of relevance for efficient water oxidation. Interestingly, the central importance of such "critical redox couples" for electrochemical WOC by transition metal oxides has already been proposed by Rasiyah und Tseung about 25 years ago [226].

6.6 Nature's metal-ion choice for WOC during the evolution of photosynthetic water oxidation

Not only amorphous manganese oxides, but also oxide materials based on cobalt and nickel can act as water-oxidation catalysts and all seem to share the same set of crucial properties with the OEC, including the option of facile oxidative self-assembly. Thus, we suggest that in the evolution of oxygenic photosynthesis, Nature could also have selected cobalt or nickel for the catalysis of water-oxidation, as they are not lacking any unique required chemical properties. On the other hand, the use of a metal like iron was not an option because the typical oxidation potentials of the $Fe^{2+} \rightarrow Fe^{3+}$ and $Fe^{3+} \rightarrow Fe^{4+}$ transitions are too low for an accumulation of oxidizing equivalents during WOC (and also not well suited for controlled oxidative self-assembly).

There is, however, one clear difference between manganese and the other two "hot candidates" cobalt and nickel: its good bio-availability, today and even more so at prebiotic times. For example, the water of lakes or rivers typically contains about 20 times more dissolved Mn (∼5 ppb) than Ni (∼0.3 ppb) or Co (∼0.2 ppb) [227]. At prebiotic times, the Mn ion concentration in seawater was most likely even more than four orders of magnitude higher than that of Co or Ni [228]. Nature's choice of manganese could therefore simply be explained by the comparably high ability of Mn^{2+} ions in the early earth's seawater compared to the only two currently conceivable "bioinorganic alternatives" cobalt and nickel (the extreme scarcity of iridium and ruthenium excludes these otherwise very well suited elements for WOC in biology). Additionally, we would like to point once again at the summary of WOC performances shown in Figure 12, which illustrates that among the earth-abundant materials, MnO_x-catalysts might be best choice for an operation at near-neutral pH-values – an important boundary condition for cellular environments. Thus, for plants and algae a manganese-based water-oxidation catalysts might represent the best compromise between bio-availability, self-assembly properties and WOC performance at pH ∼7, so that element no. 25 became the "Mighty Manganese" of oxygenic photosynthesis.

Acknowledgements: First and foremost, we thank all Ph.D. students and post-doctoral researchers of our research groups who have worked very hard over the last ∼10 years to broaden our understanding of water-oxidation catalysis by MnO_x and other transition metal oxides. On this scale, these projects only became possible due to the continuous and generous financial support of our laboratories provided via the DFG Priority Program SPP 1613 SolarH2 and the BMBF cluster project MANGAN. As both programs ended in 2019, we would like to take this opportunity to express our sincere gratitude to the coordinators of the networks at

the Technische Universität Darmstadt (SolarH2) and the Max-Planck-Institut für Chemische Energiekonversion (MANGAN) – many, many thanks for organizing these inspiring research environments!

References

1. G. Ciamician, Science **36** (1912) 385.
2. D. G. Nocera, N. S. Lewis, PNAS **103** (2006) 15729.
3. acatech – National Academy of Science and Engineering (Ed.), Articial Photosynthesis, Munich, Academy report (2018).
4. H. Dau, E. Fujita, L. Sun, ChemSusChem **10** (2017) 4228.
5. J. Messinger, W. Lubitz, J.-R. Shen, Phys. Chem. Chem. Phys. **16** (2014) 11785.
6. H. Dau, P. Kurz, M.-D. Weitze, Künstliche Photosynthese, Springer, Heidelberg (2019).
7. L. Sun, L. Hammarström, B. Åkermark, S. Styring, Chem. Soc. Rev. **30** (2001) 3649.
8. D. Gust, T. A. Moore, A. L. Moore, Acc. Chem. Res. **42** (2009) 1890.
9. M. Dinc, Y. Surendranath, D. G. Nocera, PNAS **107** (2010) 10337.
10. D. K. Bediako, B. Lassalle-Kaiser, Y. Surendranath, J. Yano, V. K. Yachandra, D. G. Nocera, J. Am. Chem. Soc. **134** (2012) 6801.
11. Y. Wu, M. Chen, Y. Han, H. Luo, X. Su, M. T. Zhang, X. Lin, J. Sun, L. Wang, L. Deng, W. Zhang, R. Cao, Angew. Chem. Int. Ed. **54** (2015) 4870.
12. G. P. Gardner, Y. B. Go, D. M. Robinson, P. F. Smith, J. Hadermann, A. Abakumov, M. Greenblatt, G. C. Dismukes, Angew. Chem. Int. Ed. **51** (2012) 1616.
13. D. K. Bediako, C. Costentin, E. C. Jones, D. G. Nocera, J.-M. Savéant, J. Am. Chem. Soc. **135** (2013) 10492.
14. H. Dau, I. Zaharieva, Acc. Chem. Res. **42** (2009) 1861.
15. N. Cox, D. A. Pantazis, F. Neese, W. Lubitz, Acc. Chem. Res. **46** (2013) 1588.
16. J. Yano, V. Yachandra, Chem. Rev. **114** (2013) 4175.
17. J. Barber, Chem. Soc. Rev. **38** (2009) 185.
18. I. Vass, S. Styring, Biochemistry **30** (1991) 830.
19. N. Cox, J. Messinger, Biochim. Biophys. Acta **1827** (2013) 1020.
20. V. Krewald, M. Retegan, N. Cox, J. Messinger, W. Lubitz, S. DeBeer, F. Neese, D. A. Pantazis, Chem. Sci. **6** (2015) 1676.
21. L. Sun, H. Berglund, R. Davydov, T. Norrby, P. Korall, A. Bo, C. Philouze, K. Berg, A. Tran, M. Andersson, G. Stenhagen, J. Ma, J. Am. Chem. Soc. **7863** (1997) 6996.
22. D. Burdinski, E. Bothe, K. Wieghardt, Inorg. Chem. **39** (2000) 105.
23. C. S. Mullins, V. L. Pecoraro, Coord. Chem. Rev. **252** (2008) 416.
24. J. D. Blakemore, R. H. Crabtree, G. W. Brudvig, Chem. Rev. **115** (2015) 12974.
25. C. Zhang, C. Chen, H. Dong, J.-R. Shen, H. Dau, J. Zhao, Science **348** (2015) 690.
26. M. Yagi, M. Kaneko, Chem. Rev. **101** (2001) 21.
27. E. Y. Tsui, T. Agapie, PNAS **110** (2013) 10084.
28. J. S. Kanady, P.-H. Lin, K. M. Carsch, R. J. Nielsen, M. K. Takase, W. A. Goddard, T. Agapie, J. Am. Chem. Soc. **136** (2014) 14373.
29. S. Mukherjee, J. A. Stull, J. Yano, T. C. Stamatatos, K. Pringouri and T. A. Stich, PNAS **109** (2012) 2257.
30. J. S. Kanady, E. Y. Tsui, M. W. Day, T. Agapie, Science **333** (2011) 733.

31. G. C. Dismukes, R. Brimblecombe, G. A. N. Felton, R. S. Pryadun, J. E. Sheats, L. Spiccia, G. F. Swiegers, Acc. Chem. Res. **42** (2009) 1935.
32. A. Llobet, Molecular Water Oxidation Catalysis, John Wiley & Sons, West Sussex (2014).
33. T. S. Glikman, I. S. Shchegoleva, Kinet. Katal. **9** (1968) 461.
34. V. Y. Sharovich, N. K. Khannanov, A. E. Shilov, J. Inorg. Biochem. **15** (1981) 113.
35. P. Kurz, Top. Curr. Chem. **371** (2016) 49.
36. S. Trasatti, J. Electroanal. Chem. **111** (1980) 125.
37. M. Morita, C. Iwakura, H. Tamura, Electrochim. Acta **24** (1979) 357.
38. J. E. Post, Proc. Natl. Acad. Sci. **96** (1999) 3447.
39. B. M. Tebo, J. R. Bargar, B. G. Clement, G. J. Dick, K. J. Murray, D. Parker, R. Verity, S. M. Webb, Annu. Rev. Earth Planet Sci. **32** (2004) 287.
40. R. M. McKenzie, Mineral. Mag. **38** (1971) 493.
41. C. E. Frey, P. Kurz, Chem. A Eur. J. **21** (2015) 14958.
42. R. Pokhrel, M. K. Goetz, S. E. Shaner, X. Wu, S. S. Stahl, J. Am. Chem. Soc. **137** (2015) 8384.
43. T. Yoshinaga, M. Sakamoto, T. Teranishi, Nanoscale **10** (2018) 10420.
44. D. M. Robinson, Y. B. Go, M. Mui, G. Gardner, Z. Zhang, D. Mastrogiovanni, E. Garfunkel, J. Li, M. Greenblatt, G. C. Dismukes, J. Am. Chem. Soc. **135** (2013) 3494.
45. E. Baktash, I. Zaharieva, C. Goebel, H. Dau, A. Thomas, Dalton Trans. **42** (2013) 16920.
46. D. Shevchenko, M. F. Anderlund, S. Styring, H. Dau, I. Zaharieva, A. Thapper, Phys. Chem. Chem. Phys. **16** (2014) 11965.
47. M. M. Najafpour, D. J. Sedigh, S. M. Hosseini, I. Zaharieva, Inorg. Chem. **55** (2016) 8827.
48. A. Indra, P. W. Menezes, I. Zaharieva, E. Baktash, J. Pfrommer, M. Schwarze, H. Dau, M. Driess, Angew. Chem. Int. Ed. **52** (2013) 13206.
49. I. Zaharieva, P. Chernev, M. Risch, K. Klingan, M. Kohlhoff, A. Fischer, H. Dau, Energy Environ. Sci. **5** (2012) 7081.
50. A. Harriman, I. J. Pickering, J. M. Thomas, P. A. Christensen, J. Chem. Soc. Faraday Trans. 1 **84** (1988) 2795.
51. F. Jiao, H. Frei, Chem. Commun. **46** (2010) 2920.
52. F. Jiao, H. Frei, Energy Environ. Sci. **3** (2010) 1018.
53. R. K. Hocking, R. Brimblecombe, L.-Y. Chang, A. Singh, M. H. Cheah, C. Glover, W. H. Casey, L. Spiccia, Nat. Chem. **3** (2011) 461.
54. C. E. Frey, M. Wiechen and P. Kurz, Dalton Trans. **43** (2014) 4370.
55. M. Wiechen, I. Zaharieva, H. Dau, P. Kurz, Chem. Sci. **3** (2012) 2330.
56. A. Iyer, J. Del-Pilar, C. K. King'Ondu, E. Kissel, H. F. Garces, H. Huang, A. M. El-Sawy, P. K. Dutta, S. L. Suib, J. Phys. Chem. C **116** (2012) 6474.
57. M. M. Najafpour, T. Ehrenberg, M. Wiechen, P. Kurz, Angew. Chem. Int. Ed. **49** (2010) 2233.
58. G. Elmaci, C. E. Frey, P. Kurz, B. Zümreoğlu-Karan, Inorg. Chem. **54** (2015) 2734.
59. I. Zaharieva, M. M. Najafpour, M. Wiechen, M. Haumann, P. Kurz, H. Dau, Energy Environ. Sci. **4** (2011) 2400.
60. M. Morita, C. Iwakura, H. Tamura, Electrochim. Acta **22** (1977) 325.
61. M. Kölbach, S. Fiechter, R. van de Krol, P. Bogdanoff, Catal. Today **290** (2017) 29.
62. E. Logothetis, K. Park, Solid State Commun. **16** (1975) 909.
63. R. N. De Guzman, A. Awaluddin, Y. F. Shen, Z. R. Tian, S. L. Suib, S. Ching, C. L. O'Young, Chem. Mater. **7** (1995) 1286.
64. D. Rogers, R. Shannon, A. Sleight, J. Gillson, Inorg. Chem. **8** (1969) 841.

65. S. M. Jasem, A. C. C. Tseung, J. Electrochem. Soc. **126** (1979) 1353.
66. P. Rasiyah, A. C. C. Tseung, J. Electrochem. Soc. **130** (1983) 365.
67. J. D. Benck, B. A. Pinaud, Y. Gorlin, T. F. Jaramillo, PLoS One **9** (2014) e107942.
68. A. Kraft, H. Hennig, A. Herbst, K. Heckner, J. Electroanal. Chem. **365** (1994) 191.
69. E. Matveeva, J. Electrochem. Soc. **152** (2005) 138.
70. M. Senthilkumar, J. Mathiyarasu, J. Joseph, K. L. N. Phani, V. Yegnaraman, Mater. Chem. Phys. **108** (2008) 403.
71. Z. N. Zahran, E. A. Mohamed, T. Ohta, Y. Naruta, ChemCatChem. **8** (2016) 532.
72. F. Zhou, A. Izgorodin, R. K. Hocking, V. Armel, L. Spiccia, D. R. MacFarlane, ChemSusChem. **6** (2013) 643.
73. M. Fekete, R. K. Hocking, S. L. Y. Chang, C. Italiano, A. F. Patti, L. Spiccia, Energy Environ. Sci. **6** (2013) 2222.
74. B. Zhang, H. Chen, Q. Daniel, B. Philippe, F. Yu, M. Valvo, Y. Li, R. B. Ambre, P. Zhang, F. Li, H. Rensmo, L. Sun, ACS Catal. **7** (2017) 6311.
75. T. Takashima, K. Hashimoto, R. Nakamura, J. Am. Chem. Soc. **134** (2012) 1519.
76. T. Takashima, K. Hashimoto, R. Nakamura, J. Am. Chem. Soc. **134** (2012) 18153.
77. S. Y. Lee, D. González-Flores, J. Ohms, T. Trost, H. Dau, I. Zaharieva, P. Kurz, ChemSusChem. **7** (2014) 3442.
78. A. Ramírez, D. Friedrich, M. Kunst, S. Fiechter, Chem. Phys. Lett. **568–569** (2013) 157.
79. A. Ramírez, P. Hillebrand, D. Stellmach, M. M. May, P. Bogdanoff, S. Fiechter, J. Phys. Chem. C **118** (2014) 14073.
80. A. Yamaguchi, R. Inuzuka, T. Takashima, T. Hayashi, K. Hashimoto, R. Nakamura, Nat. Commun. **5** (2014) 4256.
81. M. Huynh, D. K. Bediako, D. G. Nocera, J. Am. Chem. Soc. **136** (2014) 6002.
82. M. Huynh, C. Shi, S. J. L. Billinge, D. G. Nocera, J. Am. Chem. Soc. **137** (2015) 14887.
83. C. Walter, P. W. Menezes, S. Loos, H. Dau, ChemSusChem. **11** (2018) 2554.
84. M. V. Abrashev, P. Chernev, P. Kubella, M. R. Mohammadi, C. Pasquini, H. Dau, I. Zaharieva, J. Mater. Chem. A **7** (2019) 17022.
85. M. F. Tesch, S. A. Bonke, T. E. Jones, M. N. Shaker, J. Xiao, K. Skorupska, R. Mom, J. Melder, P. Kurz, A. Knop-Gericke, R. Schlögl, R. K. Hocking, A. N. Simonov, Angew. Chem. Int. Ed. **58** (2019) 3426.
86. A. Stadler, Materials **5** (2012) 661.
87. M. B. Stevens, L. J. Enman, A. S. Batchellor, M. R. Cosby, A. E. Vise, C. D. Trang, S. W. Boettcher, Chem. Mater. **29** (2017) 120.
88. R. L. McCreery, Chem. Rev. **108** (2008) 2646.
89. M. Inagaki, F. Kang, Materials Science and Engineering of Carbon, 2nd ed., Elsevier, Amsterdam, The Netherlands (2014).
90. J. Zhang, Q. Chi, S. Dong, E. Wang, Bioelelectrochem. Bioenerg. **39** (1996) 267.
91. T. F. Jaramillo, J. Bonde, J. Zhang, B.-L. Ooi, K. Andersson, J. Ulstrup, I. Chorkendorff, J. Phys. Chem. C **112** (2008) 17492.
92. A. Bergmann, I. Zaharieva, H. Dau, P. Strasser, Energy Environ. Sci. **6** (2013) 2745.
93. I. Zaharieva, D. González-Flores, B. Asfari, C. Pasquini, M. Mohammadi, K. Klingan, I. Zizak, S. Loos, P. Chernev, H. Dau, Energy Environ. Sci. **9** (2016) 2433.
94. D. González-Flores, I. Zaharieva, J. Heidkamp, P. Chernev, E. Martínez-Moreno, C. Pasquini, M. R. Mohammadi, K. Klingan, U. Gernet, A. Fischer, H. Dau, ChemSusChem. **9** (2016) 379.
95. S. Yamada, H. Sato, Nature **193** (1962) 261.

96. H. Zittel, F. Miller, Anal. Chem. **37** (1965) 200.
97. Y. Gorlin, T. F. Jaramillo, J. Am. Chem. Soc. **132** (2010) 13612.
98. H. Antoni, D. M. Morales, Q. Fu, Y. T. Chen, J. Masa, W. Schuhmann, M. Muhler, ACS Omega **3** (2018) 11216.
99. K. Mette, A. Bergmann, J. P. Tessonnier, M. Havecker, L. D. Yao, T. Ressler, R. Schlögl, P. Strasser, M. Behrens, ChemCatChem. **4** (2012) 851.
100. M. F. Mathias, J. Roth, J. Fleming, W. Lehnert, In: Handbook of Fuel Cells. Wiley, Hoboken, NJ, USA (2010), **3** P. 517.
101. S. Park, J.-W. Lee, B. N. Popov, Int. J. Hydrogen Energy **37** (2012) 5850.
102. M. G. Walter, E. L. Warren, J. R. McKone, S. W. Boettcher, Q. Mi, E. A. Santori, N. S. Lewis, Chem. Rev. **110** (2010) 6446.
103. M. Carmo, D. L. Fritz, J. Mergel, D. Stolten, Int. J. Hydrogen Energy **38** (2013) 4901.
104. J. R. Varcoe, P. Atanassov, D. R. Dekel, A. M. Herring, M. A. Hickner, P. A. Kohl, A. R. Kucernak, W. E. Mustain, K. Nijmeijer, K. Scott, T. Xu, L. Zhuang, Energy Environ. Sci. **7** (2014) 3135.
105. L. Castanheira, L. Dubau, M. Mermoux, G. Berthome, N. Caque, E. Rossinot, M. Chatenet, F. Maillard, ACS Catal. **4** (2014) 2258.
106. L. Castanheira, W. O. Silva, F. H. B. Lima, A. Crisci, L. Dubau, F. Maillard, ACS Catal. **5** (2015) 2184.
107. K. H. Kangasniemi, D. A Condit, T. D. Jarvi, J. Electrochem. Soc. **151** (2004) E125.
108. J. P. Meyers, R. M. Darling, J. Electrochem. Soc. **153** (2006) A1432.
109. J. Melder, W. L. Kwong, D. Shevela, J. Messinger, P. Kurz, ChemSusChem. **10** (2017) 4491.
110. Y. Gorlin, C. J. Chung, J. D. Benck, D. Nordlund, L. Seitz, T. C. Weng, D. Sokaras, B. M. Clemens, T. F. Jaramillo, J. Am. Chem. Soc. **136** (2014) 4920.
111. J. Scholz, M. Risch, K. A. Stoerzinger, G. Wartner, Y. Shao-horn, C. Jooss, J. Phys. Chem. C **120** (2016) 27746.
112. A. Kratzig, P. Bogdanoff, K. Ellmer, S. Fiechter, in preparation.
113. A. Kratzig, PhD Thesis, Technical University Berlin (2014).
114. B. Zhang, Y. Li, M. Valvo, L. Fan, Q. Daniel, P. Zhang, L. Wang, L. Sun, ChemSusChem. **10** (2017) 18.
115. K. S. Novoselov, A. K. Geim, S. V. Morozov, D. Jiang, Y. Zhang, S. V. Dubonos, I. V. Grigorieva, A. A. Firsov, Science **306** (2004) 666.
116. L. Xi, C. Schwanke, J. Xiao, F. F. Abdi, I. Zaharieva, K. M. Lange, J. Phys. Chem. C **121** (2017) 12003.
117. S. Heidari, J. P. Singh, H. Feizi, R. Bagheri, K. H. Chae, Sci. Rep. **9** (2019) 7749.
118. A. Ramirez, P. Bogdanoff, D. Friedrich, S. Fiechter, Nano Energy **1** (2012) 282.
119. A. Singh, D. R. Chowdhury, S. S. Amritphale, N. Chandra, I. B. Singh, RSC Adv. **5** (2015) 24200.
120. Y. Meng, W. Song, H. Huang, Z. Ren, S.-Y. Chen, S. L. Suib, J. Am. Chem. Soc. **136** (2014) 11452.
121. K. Jin, H. Seo, T. Hayashi, M. Balamurugan, D. Jeong, Y. K. Go, J. S. Hong, K. H. Cho, H. Kakizaki, N. Bonnet-Mercier, M. G. Kim, S. H. Kim, R. Nakamura, K. T. Nam, J. Am. Chem. Soc. **139** (2017) 2277.
122. K. L. Pickrahn, S. W. Park, Y. Gorlin, H.-B.-R. Lee, T. F. Jaramillo, S. F. Bent, Adv. Energy Mater. **2** (2012) 1269.
123. H. Jin, D. Hagen, M. Karppinen, Dalton Trans. **45** (2016) 18737.

124. H. S. Jeon, S. J. Ahn, M. S. Jee, S. S. Yoon, Y. J. Hwang, B. Koun, J. Electrochem. Soc. **163** (2016) 3113.
125. N. C. Strandwitz, D. J. Comstock, R. L. Grimm, A. C. Nichols-Nielander, N. S. Lewis, J. Phys. Chem. C **4931** (2013) 4936.
126. C. E. Frey, F. Kwok, D. González-Flores, J. Ohms, K. Cooley, H. Dau, I. Zaharieva, T. Walter, H. Simchi, S. Mohney, P. Kurz, Sustain. Energy Fuels **1** (2017) 1162.
127. H. Simchi, K. A. Cooley, J. Ohms, L. Huang, P. Kurz, S. E. Mohney, Inorg. Chem. **57** (2018) 785.
128. Y. Gorlin, B. Lassalle-Kaiser, J. D. Benck, S. Gul, S. M. Webb, V. K. Yachandra, J. Yano, T. F. Jaramillo, J. Am. Chem. Soc. **135** (2013) 8525.
129. Z. Morgan Chan, D. A. Kitchaev, J. Nelson Weker, C. Schnedermann, K. Lim, G. Ceder, W. Tumas, M. F. Toney, D. G. Nocera, Proc. Natl. Acad. Sci. **115** (2018) E5261.
130. Z. N. Zahran, E. A. Mohamed, Y. Naruta, J. Mater. Chem. A **5** (2017) 15167.
131. J. Melder, S. Mebs, P. A. Heizmann, R. Lang, H. Dau, P. Kurz, J. Mater. Chem. A **7** (2019) 25333.
132. K. L. Pickrahn, Y. Gorlin, L. C. Seitz, A. Garg, D. Nordlund, F. Jaramillo, S. F. Bent, Phys. Chem. Chem. Phys. **17** (2015) 14003.
133. T. Shinagawa, K. Takanabe, ChemSusChem. **10** (2017) 1318.
134. K. Klingan, F. Ringleb, I. Zaharieva, J. Heidkamp, P. Chernev, D. González-Flores, M. Risch, A. Fischer, H. Dau, ChemSusChem. **7** (2014) 1301.
135. F. Barbir, Sol. Energy **78** (2005) 661.
136. K. Sun, I. A. Moreno-Hernandez, W. C. Schmidt, X. Zhou, J. C. Crompton, R. Liu, F. H. Saadi, Y. Chen, K. M. Papadantonakis, N. S. Lewis, Energy Environ. Sci. **10** (2017) 987.
137. A. Minguzzi, F.-R. F. Fan, A. Vertova, S. Rondinini, A. J. Bard, Chem. Sci. **3** (2012) 217.
138. I. A. Moreno-Hernandez, C. A. MacFarland, C. G. Read, B. S. Brunschwig, K. M. Papadantonakis, N. Lewis, Energy Environ. Sci. **10** (2017) 2103.
139. J. Ohms, PhD-Thesis, Albert-Ludwigs-Universität Freiburg (2018).
140. Y. Mousazade, M. R. Mohammadi, P. Chernev, R. Bikas, R. Bagheri, Z. Song, T. Lis, H. Dau, M. M. Najafpour, Catal. Sci. Technol. **4** (2018) 4390.
141. A. Li, H. Ooka, N. Bonnet, T. Hayashi, Y. Sun, Q. Jiang, C. Li, H. Han, R. Nakamura, Angew. Chem. Int. Ed. **58** (2019) 16.
142. M. Rabe, C. Toparli, Y.-H. Chen, O. Kasian, K. J. J. Mayrhofer, A. Erbe, Phys. Chem. Chem. Phys. **21** (2019) 10457.
143. F. Bozoglian, S. Romain, M. Z. Ertem, T. K. Todorova, C. Sens, J. Mola, J. Benet-Buchholz, X. Fontrodona, C. J. Cramer, L. Gagliardi, A. Llobet, J. Am. Chem. Soc. **131** (2009) 15176.
144. F. Liu, J. J. Concepcion, J. W. Jurss, T. Cardolaccia, J. L. Templeton, T. J. Meyer, Inorg. Chem. **47** (2008) 1727.
145. S. W. Gersten, G. J. Samuels, T. J. Meyer, J. Am. Chem. Soc. **104** (1982) 4029.
146. H. Dau, C. Limberg, T. Reier, M. Risch, S. Roggan, P. Strasser, ChemCatChem. **2** (2010) 724.
147. W. Lubitz, E. J. Reijerse, J. Messinger, Energy Environ. Sci. **1** (2008) 15.
148. M. Görlin, P. Chernev, J. F. De Araújo, T. Reier, S. Dresp, B. Paul, R. Krähnert, H. Dau, P. Strasser, J. Am. Chem. Soc. **138** (2016) 5603.
149. M. Görlin, J. F. De Araujo, H. Schmies, D. Bernsmeier, S. Dresp, M. Gliech, Z. Jusys, P. Chernev, R. Kraehnert, H. Dau, P. Strasser, J. Am. Chem. Soc. **139** (2017) 2070.
150. M. W. Kanan, Y. Surendranath, D. G. Nocera, Chem. Soc. Rev. **38** (2009) 109.
151. Y. Surendranath, M. W. Kanan, D. G. Nocera, J. Am. Chem. Soc. **132** (2010) 16501.

152. M. Risch, K. Klingan, F. Ringleb, P. Chernev, I. Zaharieva, A. Fischer, H. Dau, ChemSusChem. **5** (2012) 542.
153. M. Suga, F. Akita, K. Hirata, G. Ueno, H. Murakami, Y. Nakajima, T. Shimizu, K. Yamashita, M. Yamamoto, H. Ago, J.-R. Shen, Nature **517** (2014) 99.
154. J.-R. Shen, Annu. Rev. Plant Biol. **66** (2015) 23.
155. M. Pérez-Navarro, F. Neese, W. Lubitz, D. A. Pantazis, N. Cox, Curr. Opin. Chem. Biol. **31** (2016) 113.
156. H. Antoni, D. M. Morales, J. Bitzer, Q. Fu, Y.-T. Chen, J. Masa, W. Kleist, W. Schuhmann, M. Muhler, J. Catal. **374** (2019) 335.
157. W. Zhang, W. Lai, R. Cao, Chem. Rev. **117** (2017) 3717.
158. M. Risch, F. Ringleb, M. Kohlho, P. Bogdanoff, P. Chernev, I. Zaharieva, H. Dau, Energy Environ. Sci. **8** (2015) 661.
159. H. Dau, L. Iuzzolino, J. Dittmer, Biochim. Biophys. Acta **1503** (2001) 24.
160. P. E. M. Siegbahn, Chem. A Eur. J. **14** (2008) 8290.
161. J. P. McEvoy, G. W. Brudvig, Chem. Rev. **106** (2006) 4455.
162. G. Mattioli, I. Zaharieva, H. Dau, L. Guidoni, J. Am. Chem. Soc. **137** (2015) 10254.
163. C. C. L. McCrory, S. Jung, I. M. Ferrer, S. Chatman, J. C. Peters, T. F. Jaramillo, J. Am. Chem. Soc. **137** (2015) 4347.
164. C. C. L. McCrory, S. Jung, J. C. Peters, T. F. Jaramillo, J. Am. Chem. Soc. **135** (2013) 16977.
165. I. Spanos, A. A. Auer, S. Neugebauer, X. Deng, H. Tu, R. Schlögl, ACS Catal. **7** (2017) 3768.
166. B. M. Hunter, J. D. Blakemore, M. Deimund, H. B. Gray, J. R. Winkler, A. M. Müller, J. Am. Chem. Soc. **136** (2014) 13118.
167. A. M. Smith, L. Trotochaud, M. S. Burke, S. W. Boettcher, Chem. Commun. **51** (2015) 5261.
168. M. W. Kanan, D. G. Nocera, Science **321** (2008) 1072.
169. F. Luo, R. Schmack, S. Ku, M. Gliech, P. Strasser, Energy Environ. Sci. **9** (2016) 2020.
170. M. A. Petit, V. Plichon, J. Electroanal. Chem. **444** (1998) 247.
171. X. Lu, C. Zhao, Nat. Commun. **6** (2015) 17.
172. M. W. Kanan, D. G. Nocera, Science **321** (2008) 1072.
173. O. Schmidt, A. Gambhir, I. Staell, A. Hawkes, J. Nelson, S. Few, Int. J. Hydrogen Energy **42** (2017) 30470.
174. E. L. Miller, R. L. Rocheleau, J. Electrochem. Soc. **144** (1997) 3072.
175. M. W. Louie, A. T. Bell, J. Am. Chem. Soc. **135** (2013) 12329.
176. A. Fallisch, L. Schellhase, J. Fresko, M. Zechmeister, M. Zedda, J. Ohlmann, L. Zielke, N. Paust, T. Smolinka, Int. J. Hydrogen Energy **42** (2017) 13544.
177. A. Fallisch, L. Schellhase, J. Fresko, M. Zedda, L. Zielke, J. Ohlmann, M. Steiner, B. Armin, S. Thiele, F. Dimroth, T. Smolinka, Int. J. Hydrogen Energy **42** (2017) 26804.
178. L. C. Seitz, C. F. Dickens, K. Nishio, Y. Hikita, J. Montoya, A. Doyle, C. Kirk, A. Vojvodic, H. Y. Hwang, J. K. Norskov, T. F. Jaramillo, Science **353** (2016) 1011.
179. O. Kasian, J.-P. Grote, S. Geiger, S. Cherevko, K. J. J. Mayrhofer, Angew. Chem. Int. Ed. **57** (2018) 2488.
180. S. Cherevko, S. Geiger, O. Kasian, A. Mingers, K. J. Mayrhofer, J. Electroanal. Chem. **773** (2016) 69.
181. K. S. Joya, Y. F. Joya, K. Ocakoglu, R. van de Krol, Angew. Chem. Int. Ed. **125** (2013) 10618.
182. D. G. Nocera, Acc. Chem. Res. **45** (2012) 767.
183. F. Urbain, V. Smirnov, J.-P. Becker, A. Lambertz, F. Yang, J. Ziegler, B. Kaiser, W. Jaegermann, U. Rau, F. Finger, Energy Environ. Sci. **9** (2016) 145.
184. B. Turan, J.-P. Becker, F. Urbain, F. Finger, U. Rau, S. Haas, Nat. Commun. **7** (2016) 12681.

185. K. Rabaey, R. A. Rozendal, Nat. Rev. Microbiol. **8** (2010) 706.
186. R. Ganigué, S. Puig, P. Batlle-Vilanova, M. D. Balaguer, J. Colprim, Chem. Commun. **51** (2015) 3235.
187. K. P. Nevin, T. L. Woodard, A. E. Franks, mBio **1** (2010) e00103.
188. N. Aryal, F. Ammam, S. A. Patil, D. Pant, Green Chem. **19** (2017) 5748.
189. S. N. Nangle, K. K. Sakimoto, P. A. Silver, D. G. Nocera, Curr. Opin. Chem. Biol. **41** (2017) 107.
190. C. Liu, K. K. Sakimoto, B. C. Colón, P. A. Silver, D. G. Nocera, Proc. Natl. Acad. Sci. **114** (2017) 6450.
191. F. Dionigi, T. Reier, Z. Pawolek, M. Gliech, P. Strasser, ChemSusChem. **9** (2016) 962.
192. J. P. Torella, C. J. Gagliardi, J. S. Chen, D. K. Bediako, B. Colón, J. C. Way, P. A. Silver, D. G. Nocera, PNAS **112** (2014) 2337.
193. C. Liu, B. C. Colón, M. Ziesack, P. A. Silver, D. G. Nocera, Science **352** (2016) 1210.
194. K. Fujimura, T. Matsui, K. Izumiya, N. Kumagai, E. Akiyama, H. Habazaki, Mater. Sci. Eng. A **267** (1999) 254.
195. N. A. A. Ghany, N. Kumagai, S. Meguro, K. Asami, K. Hashimoto, Electrochim. Acta **48** (2002) 2128.
196. J. G. Vos, T. A. Wezendonk, A. W. Jeremiasse, M. T. M. Koper, J. Am. Chem. Soc. **140** (2018) 10270.
197. F. A. Armstrong, Phil. Trans. R. Soc. B **363** (2008) 1263.
198. R. J. Debus, Biochim. Biophys. Acta **1102** (1992) 269.
199. H. Dau, M. Haumann, Coord. Chem. Rev. **252** (2008) 273.
200. D. A. Pantazis, ACS Catal. **8** (2018) 9477.
201. Y. Umena, K. Kawakami, J.-R. Shen, N. Kamiya, Nature **473** (2011) 55.
202. M. Zhang, M. Bommer, R. Chatterjee, R. Hussein, J. Yano, H. Dau, J. Kern, H. Dobbek, A. Zouni, eLife **6** (2017) e26933.
203. B. Loll, J. Kern, W. Saenger, A. Zouni, J. Biesiadka, Nature **438** (2005) 1040.
204. J. Kern, R. Chatterjee, I. D. Young, F. D. Fuller, L. Lassalle, M. Ibrahim, S. Gul, T. Fransson, A. S. Brewster, R. Alonso-mori, R. Hussein, M. Zhang, L. Douthit, C. D. Lichtenberg, M. H. Cheah, D. Shevela, J. Wersig, I. Seuert, D. Sokaras, E. Pastor, C. Weninger, T. Kroll, R. G. Sierra, P. Aller, A. Butryn, A. M. Orville, M. Liang, J. M. Holton, A. Batyuk, J. E. Koglin, S. Carbajo, S. Boutet, W. Nigel, H. Dobbek, P. D. Adams, U. Bergmann, N. K. Sauter, A. Zouni, J. Messinger, J. Yano, V. K. Yachandra, Nature **563** (2018) 421.
205. H. Bao, R. L. Burnap, Front. Plant Sci. **7** (2016) 578.
206. J. Messinger, J. H. Robblee, U. Bergmann, C. Fernandez, P. Glatzel, H. Visser, R. M. Cinco, K. L. Mcfarlane, E. Bellacchio, S. A. Pizarro, S. P. Cramer, K. Sauer, M. P. Klein, V. K. Yachandra, L. Berkeley, J. Am. Chem. Soc. **123** (2001) 7804.
207. M. Suga, F. Akita, M. Sugahara, M. Kubo, Y. Nakajima, T. Nakane, K. Yamashita, Y. Umena, M. Nakabayashi, T. Yamane, T. Nakano, M. Suzuki, Nature **543** (2017) 131.
208. G. Renger, Photosynth. Res. **92** (2007) 407.
209. T. A. Roelofs, W. Liang, M. J. Latimer, R. M. Cinco, A. Rompel, J. C. Andrews, K. Sauer, V. K. Yachandra, M. P. Klein, Proc. Natl. Acad. Sci. U.S.A **93** (1996) 3335.
210. N. Cox, M. Retegan, F. Neese, D. A. Pantazis, A. Boussac, W. Lubitz, Science **345** (2014) 804.
211. H. Dau, P. Liebisch, M. Haumann, Phys. Scr. **T115** (2005) 844.
212. H. Dau, P. Liebisch, M. Haumann, Anal. Bioanal. Chem. **376** (2003) 562.
213. P. Liebisch, L. Iuzzolino, J. Dittmer, M. Grabolle, T. Neisius, Biochemistry **44** (2005) 1894.

214. N. Schuth, I. Zaharieva, P. Chernev, G. Berggren, M. Anderlund, S. Styring, H. Dau, M. Haumann, Inorg. Chem. **57** (2018) 10424.
215. I. Zaharieva, P. Chernev, G. Berggren, M. Anderlund, S. Styring, H. Dau, M. Haumann, Biochemistry **55** (2016) 4197.
216. L. Iuzzolino, J. Dittmer, W. Dörner, W. Meyer-Klaucke, H. Dau, Biochemistry **37** (1998) 17112.
217. M. Grabolle, H. Dau, Biochim. Biophys. Acta **1708** (2005) 209.
218. H. Dau, M. Haumann, Biochim. Biophys. Acta **1767** (2007) 472.
219. D. González-Flores, K. Klingan, P. Chernev, S. Loos, M. Mohammadi, C. Pasquini, P. Kubella, I. Zaharieva, R. Smith, H. Dau, Sustain. Energy Fuels **2** (2018) 1986.
220. M. Risch, V. Khare, I. Zaharieva, L. Gerencser, P. Chernev, H. Dau, J. Am. Chem. Soc. **131** (2009) 6936.
221. M. Risch, K. Klingan, J. Heidkamp, D. Ehrenberg, P. Chernev, I. Zaharieva, H. Dau, Chem. Commun. **47** (2011) 11912.
222. D. Friebel, M. W. Louie, M. Bajdich, K. E. Sanwald, Y. Cai, A. M. Wise, M.-J. Cheng, D. Sokaras, T.-C. Weng, R. Alonso-Mori, R. C. Davis, J. R. Bargar, J. K. Nørskov, A. Nilsson, A. T. Bell, J. Am. Chem. Soc. **137** (2015) 1305.
223. M. Görlin, P. Chernev, P. Paciok, C.-W. Tai, J. F. D. Araujo, T. Reier, M. Heggen, R. Dunin-Borkowski, P. Strasser, H. Dau, Chem. Commun. **55** (2019) 818.
224. R. D. L. Smith, C. Pasquini, S. Loos, P. Chernev, K. Klingan, P. Kubella, R. Mohammadi, D. Gonza, Energy Environ. Sci. **11** (2018) 2476.
225. R. D. L. Smith, C. Pasquini, S. Loos, P. Chernev, K. Klingan, P. Kubella, M. R. Mohammadi, D. González-Flores, H. Dau, Nat. Commun. **8** (2017) 2022.
226. P. Rasiyah, A. C. C. Tseung, J. Electrochem. Soc. **131** (1984) 803.
227. J. E. Huheey, E. A. Keiter, R. L. Keiter, Anorganische Chemie, 4th ed., DeGruyter, Berlin (2012).
228. R. Williams, in: Concepts and Models in Bioinorganic Chemistry, 1st ed., H.-B. Kraatz, N. Metzler-Nolte (Eds.). Wiley-VCH, Weinheim (2006).